EXPERIMENTAL INVESTIGATION OF ELECTROPHYSICAL PROPERTIES OF HYDROGENATED AMORPHOUS SILICON

BY

MESERET YIFRU

A Thesis

Presented to the

School of Graduate Studies

and

The Faculty of Science

Addis Ababa University

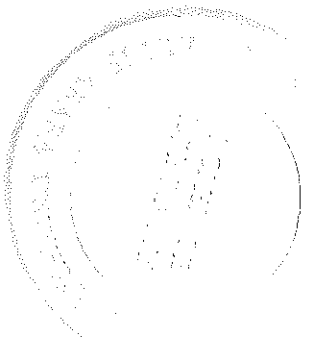

In Partial Fulfillment of the

Requirement for the Degree

Master of Science in Physics

June, 1991

ACKNOWLEDGEMENT

I would like to express my deepest gratitude to my supervisor Dr. S. BEZLUDNYI for bringing the samples from abroad, providing useful materials and for his invaluable suggestions and helps.

I should also thank my wife for her tolerance; all friends and colleagues who encouraged and assisted me in one way or another

Finally, I am very grateful to W/t Kefay Bekele who typed the thesis so carefully.

Contents

Table of Figures

Abstract

The I-V characteristics, the dc conductivity $\sigma(T)$, and the frequency dependent conductance $G(\omega)$ and capacitance $C(\omega)$ of hydrogenated amorphous silicon thin films, prepared by the HOMO CVD method, are reported. A temperature and applied voltage range dependent nonlinear I-V characteristics was obtained for films with sodium substrate. The temperature dependent dc conductivity was found to obey the band conduction model for the 296-417K temperature range. The frequency dependent conductance $G(\omega)$ exhibited a nonlinear frequency dependence. $G(\omega)$ showed a large temperature dependence and its frequency exponent S found to decrease with increasing temperature. The ac results, being analyzed with reference to five models of ac conductivity in amorphous semiconductors, agreed with the correlated barrier hopping model for the 10KHZ-1MHZ frequency range.

Introduction

The theoretical ideas used to treat crystalline solids has been long found inadequate to amorphous solids. The essential aspect with which the structure of amorphous solids differs from that of their crystalline counter parts is the absence of long-range order in the first that leads to absence of translational periodicity.

There are a number of technological applications in which amorphous solids have an advantage over the crystallines. Whenever an amorphous solid can be used in place of a crystalline one in an application calling for large area sheets or films, it is generally advantageous to do this and thereby avoid the expense of preparing large area single crystals.

Xerography is the most widely used form of electrophotography or electrostatic imaging which is the basis of most plain-paper copying machines used in offices, libraries, etc., and at the heart of the process is a large-area thin film photoconducting element which is an amorphous semiconductor.

The Ultimate application of large-area photoreceptor films is clearly in the field of solar energy. Amorphous silicon (a-S_i) is an interesting long-term candidate for solar-cell technology. Eventhough crystalline silicon, of course, is of overwhelming importance in the electronic industry, amorphous silicon can

be prepared in large-area films at a far lower cost than its crystalline counterpart. Here it is better to note that the material of interest with respect to solar-cell technology is not pure amorphous silicon but is instead an amorphous silicon containing appreciable hydrogen (usually written as a-S_i:H).

Some properties of amorphous semiconductors are not yet understood. It was reported [11, 23] that the properties of these materials are sensitive functions of the preparation conditions. The prospect of low cost semiconductor devices, in particular solar cells, has stimulated a diverse research work in the field of amorphous semiconductors. The absence of a general frame work to study amorphous semiconductors forced theoreticians to deal with highly idealized models in order to describe particular phenomena in these materials.

Hoping to contribute something to the science of amorphous semiconductors, the aim of this work was to investigate some properties of hydrogenated amorphous silicon films prepared by the HOMO CVD method under dark condition and ultraviolet illumination and with sodium and corning glass substrates. In the first two chapters a brief review of the literature about amorphous semiconductors, in particular amorphous silicon, was presented. The third chapter is about the whole experimental techniques and procedures taken in getting experimental results. The results of measurement on I-V characteristics, temperature dependent electrical conductivity and ac losses are discussed in the fourth chapter.

1 ELECTRONIC STATES AND NONDISPERSIVE TRANSPORT

1.1 Localization

According to Band-theory there exist a set of stationary states available to any one electron, and that all of the electrons are distributed among these states according to Fermi-Dirac Statistics. These states ψ_{nk} are given by the solutions of the Schrodinger equation $H\psi_{nk} = E_{nk}\psi_{nk}$. For crystals the potential V, which is intended to account for the interaction of one electron with all of the other particles in the crystal (and therefore the Hamiltonian H), is periodic in space with the translational periodicity of the crystal structure. It then follows that the wavefunctions ψ_{nk} are Bloch functions of the form $e^{ikx}\ U_{nk}(x)$. The quantum numbers characterizing each wavefunction are the wave-vector k, an integer band index n, and the energy eigenvalue E_{nk} or $E_n(k)$. The functional form of the dependence of $E_n(k)$ upon the crystal momentum (hk) for each band (n) specifies the electronic energy band structure of a crystalline solid. Each band can accomodate 2N electrons, where N is the number of unit cells in the crystal and the factor 2 arises from the spin degeneracy.

In the Bloch theory of electrons in crystal, a solid is an insulator if each band is either completely filled or completely empty. The Fermi energy, E_F, lies between bands and there is an energy gap separating the highest lying filled (valence) baand and the lowest-lying empty (conduction) band.

The electronic wavefunctions corresponding to extended states (i.e., conduction or valence bands) have appreciable amplitude throughout the solid. For crystals these are Bloch functions. But the validity of Bloch function solutions depends upon the presence of long-range order. Since there is absence of long-range order, there is no meaning of $E_n(k)$ energy band diagram for electronic states in amorphous solids. Although extended electronic states are present [1] and important in these solids, they cannot be characterized by quantized wave-vector values as in crystals (i.e., k is not a good quantum number in amorphous solids).

Unlike crystals, in amorphous solids there exist electron states in the energy gap between the valence and conduction bands. These states are called localized states and are described by localized wavefunctions. The meaning of a localized state is indicated by Fig. 1.1b [1,page 226] . A localized electron wavefunction is concentrated near a center composed of just few

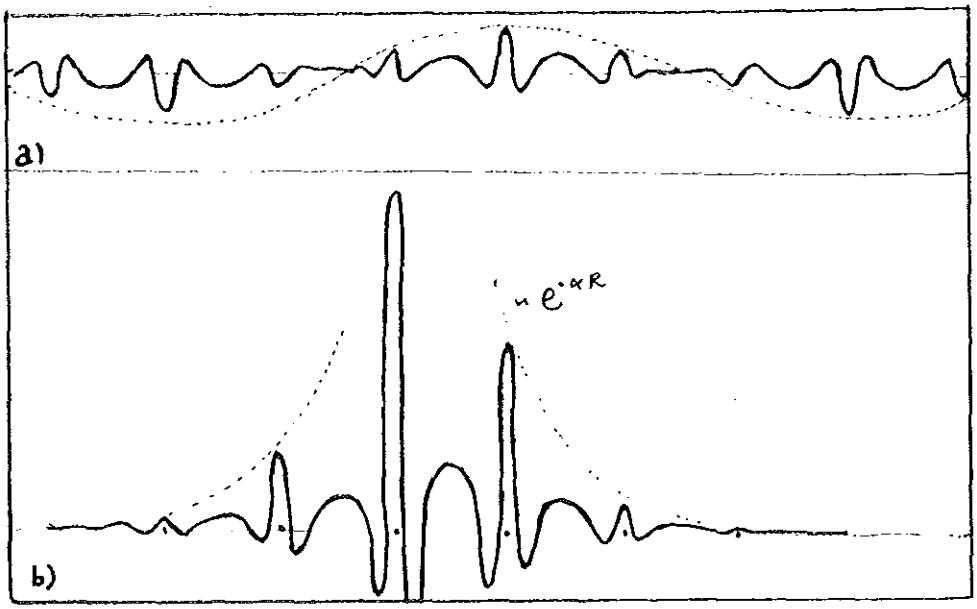

Fig.1.1 Distinction between a) extended and b) localized electron wave functions.

atoms, and has negligible amplitude elsewhere in the solid. It's amplitude spatially decays away exponentially with distance R, from the localization center, as $e^{-\alpha R}$. The quantity α, an important parameter for a given localized state, is known as the inverse localization length.

In amorphous solids the potential wells representing the atomic sites are no longer all the same. Instead of a single well depth (and bound-state level) as in the crystalline case (Fig. 1.2a) there is a random distribution of well depths (and corresponding levels) in the amorphous case schematicized in Fig. 1.2b. The width of the distribution which specifies the energy range of the disorder-induced spatial fluctuations of the potential energy seen by an electron at the atomic sites is denoted by W.

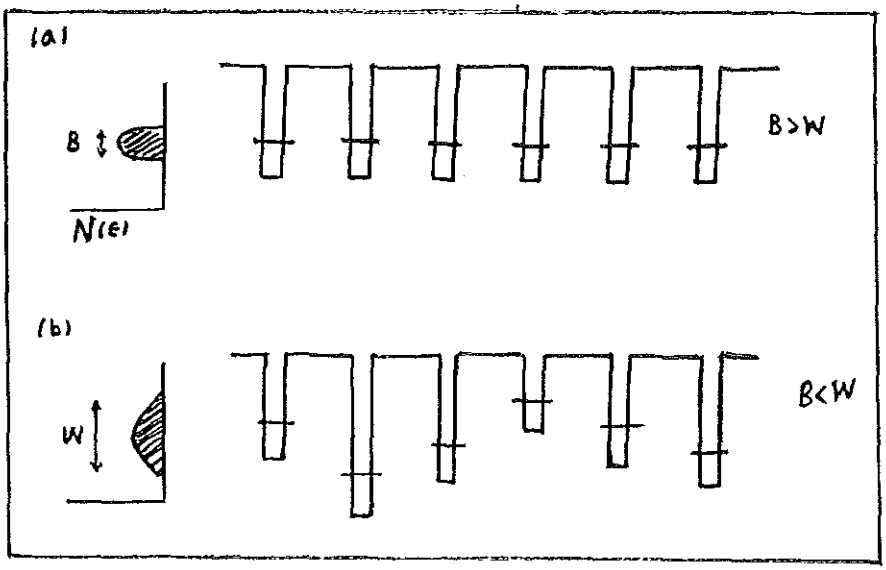

Fig. 1.2 One-electron tight-binding picture (a) with little potential fluctuation (b) with large potential fluctuation. When the width W of the disorder exceeds the overlap bandwidth B, disorder-induced localization takes place.

Anderson [2] in 1958 showed that when the dimensionless disorder parameter W/B (Fig. 1.2b) is sufficiently large (exceeded a critical value which later work showed to be of order 2 [3,5]), all the states in the valence band are localized. This notion of disorder-induced localization was subsequently extended by Mott and others [1, page 233] in a way that has strongly influenced current thinking about electronic states in amorphous semiconductors. When the disorder is great enough for W/B to satisfy Anderson's criterion, all of the states in the band become localized. Mott pointed out that even for smaller degrees of disorder, states in the tail of the band are localized. This feature of electrons in amorphous solids is indicated on the density-of-states diagram shown in Fig. 1.3. The energies for which states are localized (the shaded regions) correspond to the tails at the top of the valence band and bottom of the conduction band. Within the main body of each band,

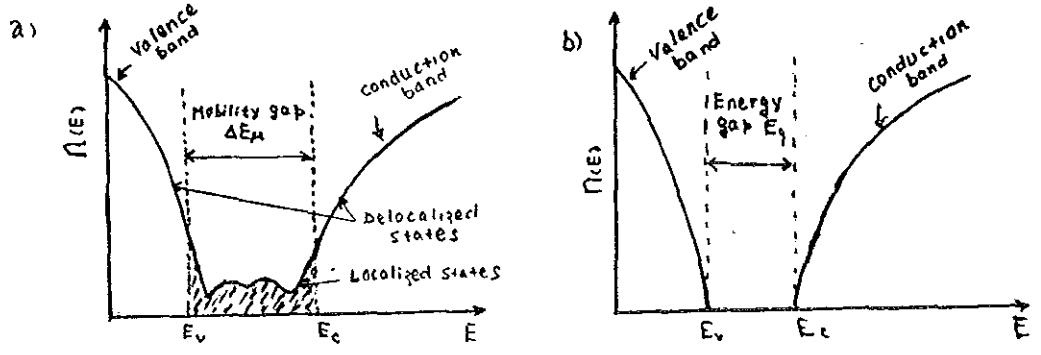

Fig. 1.3 Schematic showing the density of state function n(E) for an amorphous (a) and for a crystalline (b) solid.

the states are extended. The demarcation energies separating regions of localized and extended states are referred to as mobility edges.

Localized gap states are very important in semiconductors and insulators since they can serve as sources (doping) or sinks (recombination centres, trapping sites) for electrons and holes in the bands.

1.2 States in the gap due to defects

As we have seen in the last section so called localized states as a result of specific defects, may exist in the gap, and do in amorphous semiconductors. These states in amorphous materials are essentially of two types [4] , intrinsic and extrinsic. The intrinsic localized states are defined as those arising from the distribution of bond angles and interatomic distances statistically occuring in an amorphous solid and the extrinsic localized states are defined as those arising from defects (broken chemical bonds) and impurities (as in crystalline solids). Intrinsic localized states are expected to be the principal contribution to the localized states occuring near the band edges; defect states on the other hand are belieyed to be the source of the large density of localized states typically seen over the remainder of the gap in many amorphous materials.

Davis and Mott (1970) [3] suggested that in non-crystalline semiconductors the Fermi energy could be pinned at defect states, and Mott (1972) proposed that the pinning was by two charge states of the same defect, the level being broadened by disorder and separated by the Hubbard $U(< \frac{e^2}{Kr_{12}} >)$ for two electrons in the defect (i.e., the average of the interaction energy between a pair of electrons on a single site). This is illustrated in Fig. 1.4. If the two bands overlap, the following are predicted results;

a) The Fermi energy is 'pinned' and so will vary only slowly with doping;
b) Variable-range hopping conduction can occur, charge transport taking place through the motion of electrons within a few multiples of KT from the Fermi energy;
c) AC conduction according to the mechanism of Pollak and Geballe (1961) [16] will occur.

As we will see in section 1.5 the localized gap states in a-S_i, now generally believed, [5] are consequences of 'dangling bonds'-that is points in the silicon network where there is a three-fold coordinated Silicon atom, so that one of the four S-P bonds contains only a single electron. Recent [6] calculations of the electronic states of hydrogenated a-S_i have demonstrated the existence of dangling-bond states in the gap.

The dangling bond carrying a single unpaired electron acts as a deep donor [5] ; it can give up its electron to the conduction band. The energy levels of such states are thought to be

broadened by the random arrangment of atoms from site to site. Thus in the plot of the density of states shown in Fig. 1.4, these donors will contribute to the peak marked D. But singly occupied dangling bond centers can also act as acceptors, since an electron can be raised from the valence band and put onto

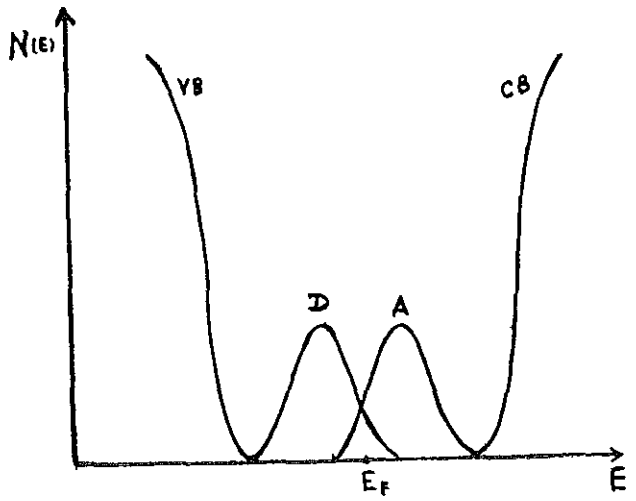

Fig. 1.4 Density of states in hydrogenated amorphous silicon, showing two bands of localized states (D and A) caused by dangling bands [5]

the site, resulting in double occupation. So the possible energies of an extra electron are marked on the diagram as A. The difference between the energies D and A is the Hubbard energy U. For amorphous silicon containing hydrogen it seems to be about 0.7eV. It is assumed that the broadening is great enough to ensure that the two bands overlap. This will mean that, in equilibrium, some of the states will carry two electrons and some none. Electron states, as in a metal, will be occupied up to a limiting energy, which we denote by E_F, the Fermi energy. The density of states, $N(E_F)$ is non zero, because of the overlap.

As regards the density of defects in deposited films, and thus for all forms of amorphous silicon, the problem of what determines the concentration is difficult. N.F.Mott [3] suggested that the concentration is a function of the rate and temperature of deposition, but that under condition when the film is amorphous $10^{19}cm^{-3}eV^{-1}$ is, in Silicon, the lowest limit. From the work of Huag et al. [22] a midgap density of states as low as $2x10^{16}cm^{-3}eV^{-1}$ is possible for hydrogenated a-S_i.

1.3 Mobility

Since the localized state density is so large in many amorphous semiconductors they have no true energy gap. Transport via these gap states is possible [4] ; i.e., an electron can move from one localized site to another. But this would give rise to small mobilities compared to transport involving the delocalized (extended) states. Hence there is a mobility gap, seen in Fig. 1.3a, rather than an energy gap. This mobility gap is expected to have sharp boundaries E_c and E_v which serve as the demarcation between localized and delocalized states. The mobility gap ΔE_μ is a little bigger than ΔE, the forbidden energy gap for crystalline material [7] .

According to the work of Lecomber and Spear [9] the transport mechanism can be divided into three temperature regions. For

higher temperatures (T>240K) the transport mechanism is an activated process with activation energy ΔE. It was suggested [9] the electrons drift in the extended states, near E_c; during the transit they interact with the localized states through trapping and thermal release. The total time a carrier spends in localized states is included in the measured transit time, leading to a trap-controlled drift mobility μ_D, which is related to the mobility μ_o near the bottom of the extended states by an expression of the form

$$\mu_D = \mu_o \alpha \exp[-(E_c - E)/KT] \qquad (1.1)$$

where α is a factor that depends on the form of localized state distribution.

From the work of Lecomber and Spear [9] the magnitude of μ_o supports the model that was already suggested by Cohen and Mott. These suggest a transport mechanism through delocalized (extended) states near E_c for which the mean free path is of the order of the interatomic separation a. The transport may be likened to Brownian motion and an approximate upper limit to the mobility given by

$$\mu_o \leq (e\ a^2/6KT)\nu_{el} \qquad (1.2)$$

where ν_{el} is a typical electronic frequency ($\sim 10^{15}$ HZ). This equation predicts that $\mu_o \tilde{} 5 Cm^2\ Sec^{-1} V^{-1}$ at room temperature.

With decreasing temperature, the probability of thermal release from a localized state becomes rapidly smaller, and eventually hopping by the trapped electron to a neighboring site will become the predominant transport mechanism. In all probability these sites are not at the same energy. Consequently the transport is interpreted as a phonon-assisted hopping between localized states lying in the energy range from E_c to the lowest lying state in the distribution of the localized states.

It follows that a hopping mobility μ_L is expected to be of the form [4]

$$\mu_L(E) = \mu_o(E) e^{-W(E)/KT} \qquad (1.3)$$

where the quantity W is the activation energy. It can be argued that μ_L is such that

$$\mu_L < 0.1 - 1.0\ cm^2\ Sec^{-1}\ V^{-1} \qquad (1.4)$$

the pre-exponential term in Equ.(1.3) is [8]

$$\mu_o = \left(\frac{eR^2}{6KT}\right)\nu_{ph} \qquad (1.5)$$

where ν_{ph} is the phonon frequency and R is the distance covered in one hop. At very low temperatures a variation of Eqn. (1.3) is expected [4] for those localized states near E_F;

$$\mu_L(E) = \mu_0(E) e^{-C/T^{1/4}} \qquad (1.6)$$

This temperature dependence arises since electrons are forced to tunnel longer distances to sites with energies closer to their initial energy due to the lack of phonons at low temperatures.

1.4 Conductivity

As we have mentioned in the last section electrical conduction processes in amorphous semiconductors can be classified into three catagories corresponding to different temperature ranges [8] :

a) at high temperatures carriers are excited across the mobility gap into the extended states (band conduction)

b) at intermediate temperatures carriers are excited into localized states of the band tails through hopping transport (i.e., thermally activated nearest neighbor hopping)

c) at very low temperatures, thermally assisted tunneling between states at the Fermi level is responsible for conduction.

The temperature dependence of the conductivity for band conduction obeys the Arrhenius relation [12]

$$\delta = \delta_o \exp(-\Delta E/KT) \qquad (1.7)$$

Where ΔE is the activation energy. For films of a-SiH which show band conduction ΔE = 0.5-0.9eV and the pre-exponential constant $\delta_{o\sim} 10^3\ \Omega^{-1}\ cm^{-1}$ [12]. This activated band conduction ($\log \delta \sim T^{-1}$) was observed [12] at high temperatures in undoped amorphous silicon films containing about 5-10 at % hydrogen prepared by magneto reactive sputtering.

The transport in a-Si and a-SiH having high density of gap states would be characterized by a large contribution from hopping between localized states, which may involve the whole range of energies of the mobility gap. For transport due to activated nearest neighbor hopping an equation similar to Eqn. (1.7) applies with smaller values for the hopping energy (~0.1 eV) with a preexponential constant ($\lesssim 1\ \Omega^{-1}\ cm^{-1}$).

Mott's variable-range hopping treats transport by phonon-assisted tunneling of electrons between sites in a system where E_F lies in a uniform density of states in an infinite solid. Two hopping transitions are schematically indicated [1] by A and B in Fig.1.5, two possible tunneling processes which take an electron in a filled state below the Fermi level to either of two nearby empty states above E_F. R denotes the distance the electron hops, while W denotes the energy separation of the final and initial states. Since energy-lifting hops must occur for this tunneling mechanism to contribute to the

macroscopic dC conductivity, and since phonons must be around to supply energy for such hops, the hopping conductivity is finite at finite temperature but vanishes at zero temperature.

For thick films (>500Å in thickness) it is expected that the temperature dependence of the phonon- assisted quantum mechanical tunneling transport mechanism obey the relation [12,1]

$$\delta = \delta_o \exp\left[-(T_o/T)^{1/4}\right] \qquad (1.8)$$

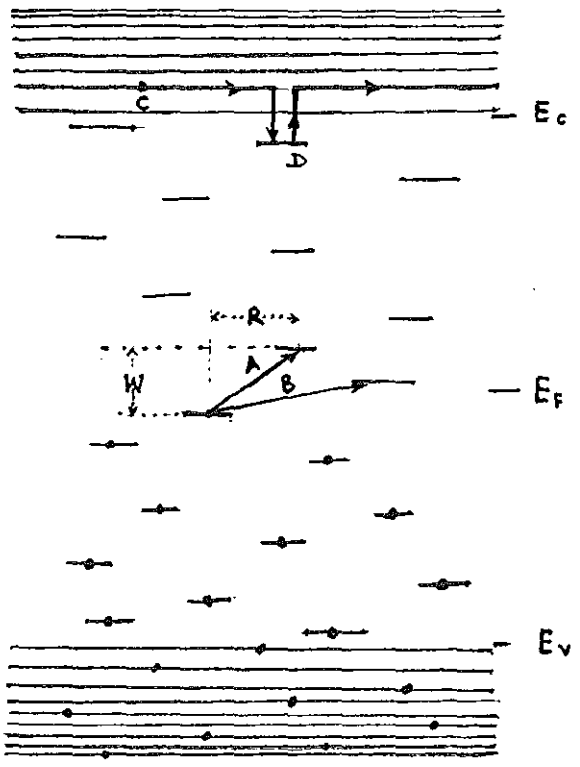

Fig. 1.5 Energy-level schematic for electronic conduction mechanisms in an amorphous semiconductor.[1,Page 276]

where [12]

$$T_o = \frac{18\alpha^3}{KN(E_F)} \qquad (1.9)$$

and α^{-1} is the extent of the localized wave function, $N(E_F)$ is the density of states (or hopping sites) at the Fermi level and K is the Boltzmann's constant.

Mott's intuitive argument for the "$T^{1/4}$ law" proceeded from the approximate expression for the R,W,T dependence of the probability of the occurrence of an energy-upward hop (such as A or B in Fig. 1.5) of distance R and energy W taking place at temperature T. Mott emphasized that there exist a trade-off between hopping distance R and mismatch energy W which implies that the nature of the dominant (i.e., most likely) hops necessarily changes with temperature. It is possible to understand this by carefully examining Fig. 1.5 and comparing the hopping probabilities of A and B as the temperature decreases to zero. It is clear that the lower the temperature, the more difficult it is to overcome a given barrier W and the more desirable it is for the electron to hop further to find a lower W.

It was shown [1] that the approximate expression for the most probable hopping distance, R, is

$$R \simeq [\alpha KTN(E_F)]^{-1/4} \qquad (1.10)$$

This shows how the hopping range changes with temperature, hence "variable-range hopping."

1.5 Hydrogenation and Doping

One of the characteristics of most amorphous semiconductors is a high density of localized states in the normally forbidden energy gap. For so long a time it was believed that unlike their crystalline counterparts it is impossible to dope amorphous semiconductors such as silicon. The reason believed [8] for this resistivity to doping is:

a) that the dopant atoms would take up their normal valence rather than the tetrahedral bonding of the host material due to the flexibility of the random network of the amorphous state.

b) the density of states in the gap of most amorphous semiconductors due to band tailing or structural defect is sufficiently high, as evidenced by electron spin-resonance experiment, that the Fermi level remains pinned at the centre.

Chittick et al (1964) [11,4] produced a hydrogenated amorphous silicon, a-SiH, by glow-discharge decomposition of silane (SiH_4). Subsequent investigations by other group, have shown that a substantial proportion of hydrogen is incorporated into the amorphous silicon and that, as a consequence, the properties of the material are markedly changed.

The primary role of hydrogen pointed out by Lewis et al (1974) [1] is to replace a dangling bond by a Si-H bond. Hydrogen is present from 3% upwards in amorphous silicon prepared by

the glow-discharge deposition of silane. It is located as = Si-H bonds and also $=Si-H_2$ and $-Si-H_3$. Thus hydrogen removes the gap states associated with the dangling bonds. In addition [1], to compensating dangling bonds hydrogen evidently opens up the weak reconstructed bonds associated with the voids and bonds to those silicon atoms as well, replacing each such long Si-Si bond by two Si- H bonds. Since the Si-H bond is very strong and its bonding antibonding splitting is larger [1] than that of Si-Si, the states introduced by the Si-H bonds lie at energies which are outside of the band gap region of the a-Si "host." The effect of all of this is to wipe out most of the electron states in the gap which the network defects native to a-Si would normally introduce.

Calculations, done by A-D.Zdetsis et al [6] , on the electronic states of hydrogenated a-Si gave evidences for what we discuss above. The existance of dangling-bond states in the gap is demonstrated. 'It is also shown the restoration of the band gap E_g upon hydrogenation and its widening mainly to be due to the recession of the valence band. The extension of these calculations, also, showed that the optical gap is larger than the DOS gap.

In general hydrogenated amorphous silicon films are more resistive than a-Si films without hydrogen. As we have seen, this is for hydrogen compensates dangling bonds which are major sources of localized states in the gap. N. Savvids [12]

showed that the conductivity of a-SiH thin films, prepared by magneto reactive sputtering, reduces for specimens with concentration of up to 5-10 at% hydrogen. But films containing more concentration, 15-30 at%, show increasing overall conductivity with increasing hydrogen content and this shows that H-induced defects are created in the gap. It is believed that high concentration of hydrogen causes H-induced defects which give rise to increasing defect-related density of states in the gap. Consequently, extrinsic properties which characterize a-Si, for example, variable-range hopping conductivity and tailing of the optical absorption edge may also be found in H. rich a-SiH (also called H-rich alloy).

Though it was assumed that amorphous semiconductors could not be doped, in 1975 Spear and LeComber [5] showed that thin films of a-Si deposited from a glow discharge could be doped both n-type and p-type. Like for the crystal, this can be done by the incorporation of phosphorus and boron for n- and p-type doping, respectively. The threefold coordination of the dopant will be electrically non-active whereas the fourfold one acts like in the doping of the crystal.

It was observed [5,12] that conductivity increases with increasing doping. Also from the work of N. Savvides [12] it was found that the values of σ_o , T_o and thus $N(E_F)$ of Eqns (1.8, 1.9) markedly changes with doping. These results thus confirm that doping certainly enhances the density of gap states.

2 AC LOSS AND MODELS

2.1 The Frequency-Dependent Loss Measurement as Applied to Amorphous Semiconductors

The measurement of the real and imaginary parts of the frequency-dependent response of a sample is a well stablished technique in the study of the solid state. Among the well established techniques in the literature describing the a.c. response of amorphous semiconductors is the measurement of the real and imaginary components of conductivity σ_1 and σ_2, respectively.

The importance of frequency-dependent loss measurements in illuminating the physics of amorphous semiconductors arises because the a.c. conductivity is often dominated by electron states deep within the principal energy gap, in the region of the Fermi level. Such deep defect states are invariably associated with the irregularities and discontinuities of these materials. In some, such as the pure tetrahedral semiconductors silicon and germanium, as we mentioned in Chapter 1, the density of these defects is so high that the electron transfer processes between them dominate the transport, especially at low temperatures.

Alternating current loss measurements are an important means by which deep defect centers may be studied. They are sensitive to processes in which such centres or group of centres, develop electron dipole moments under the action of the applied

field. The simplest such process to consider, and one which dominates the theoretical literature, involve a pair of centres in close proximity. When an electric field is applied the relative invironment of the pair of centres changes and this causes transition between them and thus a net polarization will occur. The time taken for this to occur is called the intrinsic relaxation time of the pair, τ .

The rate of polarization can be detected as a current in an ac experiment. The resultant loss is dominated [7] by pairs having relaxation times around ω^{-1}, the reciprocal of the angular frequency of the applied field. It is clear that the random distribution of environments ensures that a wide range of relaxation times will in general be found, and hence the study of a.c. losses can give important information about the number and distribution of centers.

2.2 General Basis of Relaxation Loss due to Electron Processes.

If an electron is constrained to hop between pair of states the effect [25] is that of a fluctuating dipole which contributes to the a.c. conductivity. The approach which is frequently adopted [17] in calculating a.c. loss is to sum up the losses due to such pairs to obtain the overall response of a bulk sample. This is generally known as the pair approximation. Usually this approach is started from the model calculation first analyzed by Pollak and Geballe [16] for a pair of single electron states 1 and 2 separated in energy by an amount Δ and in space by a distance R (figure 2.1).

When a sinusoidal perturbing electric field E of angular freq-

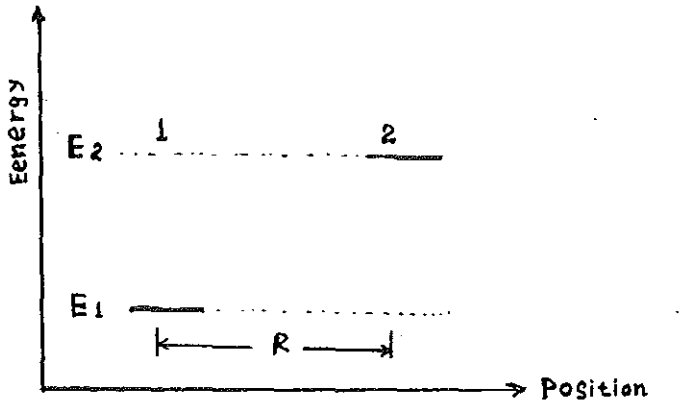

Fig. 2.1 Parameters for a pair of states 1 and 2

uency ω is applied in the direction of R the energy splitting decreases by an amount eER. Assuming that the states are occupied by only one electron, according to the summary given by A.R. Long (1982) about what was derived by Pollak and Geballe (1961), the polarizability of the state for a small field (eER <<KT) was given as

$$\alpha = \frac{e^2R^2}{4KT} \cdot \frac{1}{\cosh^2(\Delta/2KT)} \cdot \frac{1}{1+i\omega\tau} \qquad (2.1)$$

where the effective relaxation time τ is given by

$$\tau = \frac{\tau_o}{2} [\mathrm{Cosh}\ (\Delta/2KT)]^{-1} \qquad (2.2)$$

From Eqn (2.1) we see that the respons has a Debye form $(1/1+i\omega\tau)$, with an imaginary part which peaks at $\omega \sim \tau^{-1}$ and also the factor $[\cosh(\Delta/2KT)]^{-2}$ ensures that loss will occur for pairs where the states are separated in energy by $\leq KT$.

2.3 Application and Validity of the Pair Approximation

In section 2.2 we have calculations that are valid in the case of an isolated pair of states which is singly occupied and essentially uncoupled to any surrounding states. However in most realistic models of amorphous semiconductors a broad spatial distributions of electronic states in the region of the Fermi level are proposed, and the applicability of the pair approximation to such cases needs to be carefully considered.

It is assumed [16,17,26] that the coupling between the centers of a pair decreases with their separation, the corollary being that the relaxation time is an increasing function of the separation, R. Hence for a random distribution of states in space those pairs of states which happen to lie close together will have the shortest relaxation times, and thus, according to the results of section 2.2, respond at the highest frequency. These pairs are unlikely to lie equally close to other states, and hence at such frequencies they will be decoupled from their surroundings and the pair approximation should work. Interaction with other states merely serves to establish the mean number of electrons in the pair. It is therefore deduced that the pair approximation is likely to work best at high frequencies where the states which contribute to the loss are closely spaced.

As the frequency of measurement is lowered then the separation between states which can contribute to the a.c. loss will rise and interactions between the contributing pairs and other states

surrounding them will become important. At this stage the pair approximation is likely to fail. It is possible to make an estimation for the condition of pair approximation validity, interms of the number density of contributing states to the loss.

If the number density of states contributing to the loss is N, then their mean separation is $\sim N^{-1/3}$. The pair approximation then holds for separations less than the mean separation. If the length of transfer process associated with loss at a particular frequency according to the pair approximation, R_w, is greater than or of the order of $N^{-1/3}$, then due to the coupling with the surrounding the pair approximation is likely to be inadequate. Conversely, the lower the value of N, the greater the accuracy of the pair approximation and the larger the range over which it can be applied.

Assuming a uniform distribution of electron states in space (with N states per unit volume) and in energy over a range Δ_0, the single particle density of states within this band g_0 is N/Δ_0. Considering a pair of states, E_1 and E_2, each state can be occupied by up to two electrons of opposite spin, but because of the interactions between two electrons on localized states the energy of the second electron will not normally be the same as the first. We write it in the form E_1+U, where U is the intrasite correlation energy, which is assumed to be the same for both sites.

Assuming that $U>>\Delta_0$ and the energy, E_{12}, due to intersite correlation, which is a function of R, is zero for a small sinusoidal perturbing field the expression derived [17] for the polarizability, of a pair of states E_1 and E_2, is

$$\alpha(E_1,E_2,R) = \frac{e^2R^2}{4KT} \cdot \frac{1}{\mathrm{Cosh}[\beta/2(E_1-E_2)]\{\cosh[\beta/2(E_1+E_2)] + \cosh[\beta/2(E_1-E_2)]\}} \times \frac{1}{1+i\omega\tau} \qquad (2.3)$$

where $\beta=1/KT$

After integrating the polarizability over all possible states 2 surrounding a given state E_1 so as to obtain the average polarizability, the complex conductivity becomes

$$\sigma = \frac{\pi}{6} e^2\beta g_0^2 \iiint R^4 \frac{i\omega}{1+i\omega\tau} \times \frac{dRdE_1dE_2}{\cosh[\beta/2(E_1-E_2)]\{\cosh[\beta/2(E_1+E_2)] + \cosh[\beta/2(E_1-E_2)]\}} \qquad (2.4)$$

which includes both the real and imaginary components that we shall use in the coming sections.

2.4 Models for Frequency-Dependent Conductivity

A frequency-dependent (ac) electrical conductivity has been observed in many amorphous semiconductors and invariably has the form

$$\sigma_{ac}(\omega) = A\omega^{s} \qquad (2.5)$$

where the frequency exponent S is less than or equal to unity.

Many different theories for ac conduction in amorphous semiconductors have been proposed in the past. It is commonly assumed that the "pair approximation" holds; namely, the dielectric loss occurs because carrier motion is considered to be localized within pairs of sites. In essence, two distinct processes have been proposed for relaxation mechanism, namely quantum mechanical tunneling (QMT) or classical hopping over a barrier (or some combination or variant of the two) and it has been varously assumed that electrons or atoms (carrying at least some charge) are the carriers responsible.

In these models the a.c. conductivity is calculated within the pair approximation. The dependence of the loss on physical parameters of the system helps to compare theory and experiment. The comparision of the a.c.conductivity, for a particular model, with Eqn.(2.5) allows to determine the frequency exponent,S,of the frequency-dependent conductivity.

For single-electron motion undergoing QMT, it was shown that [17,18]

$$S = 1 + \frac{4}{[\ell n(\omega\tau_{o})]} \qquad (2.6)$$

showing that the model predicts that the frequency exponent s to be temperature independent, but frequency dependent.

A temperature-dependent frequency exponent can be obtained within the framework of the QMT model by assuming that the carriers form nonoverlapping small polarons, i.e., the total energy of a charge carrier is lowered by the polaron energy W_p. In this case the frequency exponent of $\sigma(\omega)$ is given [17,18] as

$$S = 1 + \frac{4}{\ell n(\omega\tau_{op}) + W_H/KT} \qquad (2.7)$$

where W_H is the polaron hopping energy. This expression shows that S is temperature dependent.

It is assumed that relaxation also occurs by hopping over a barrier. In the case of hopping over a barrier for which the barrier height W is correlated with the intersite separation as a result of the coulombic interaction between the charge carrier and the charged-defect centers we have the so called "correlated barrier hopping," CBH. In this model the frequency exponent S was evaluated [17,18] to be

$$S = 1 - \frac{6KT}{W_m + KT\ell n(\omega\tau_o)} \qquad (2.8)$$

where W_m is the maximum barrier height (assumed to be constant for all centers).

In the case of large polaron tunneling, where the large polaron wells of two sites overlap, thereby reducing the value of the polaron hopping energy, $W_H = W_{Ho}(1-\gamma_o/R)$, where γ_o is the polaron radius, the frequency exponent S of $\sigma(\omega)$ is given [17,18] as

$$S = 1 - \frac{8\alpha R_\omega + 6\beta W_{Ho}(\gamma_o/R_\omega)}{2\alpha R_\omega + \beta W_{Ho}(\gamma_o/R_\omega)^2} \qquad (2.9)$$

where α is the inverse localization length.

Figure 2.2 shows the temperature dependence of the frequency exponent S of the ac conductivity predicted by various models. Thus if one is able to determine the temperature dependence of S for a particular sample it is possible to draw a conclusion as to the likely mechanism of charge transport.

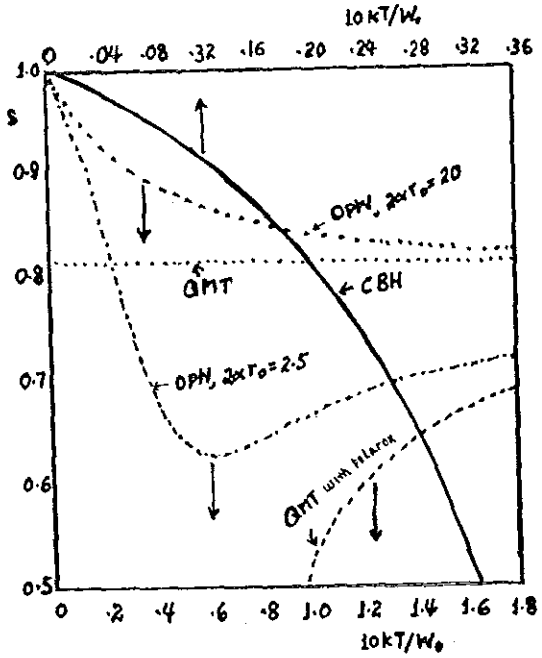

Fig. 2.2 Temperature dependence of the frequency exponent S of the ac conductivity predicted by various models and plotted versus reduced temperature KT/W_o. (OPW-overlapping-large-polaron) [18]

2.5 The Correlated Barrier Hopping (CBH) Model

As it was mentioned in last section one of the models for the electron coupling between pairs of deep defect states close to the Fermi level is the correlated barrier hopping (CBH) model. In this model a charge carrier of the pair is considered to thermally activated over the potential barrier separating them. This model was first introduced by Pike [19] to account for ac loss in scandium oxide films.

If we consider a single electron hopping between positive defect centers then the potential barrier will be reduced by the Coulombic interaction (Fig.2.3), and the barrier height W is correlated with the separation R according [17] to

$$W = W_m - \frac{e^2}{\pi\varepsilon\varepsilon_o R} \qquad (2.10)$$

where ε is the dielectric constant of the material and W_m is the energy required completely to remove the electron from the site into extended states (i.e., the maximum barrier height).

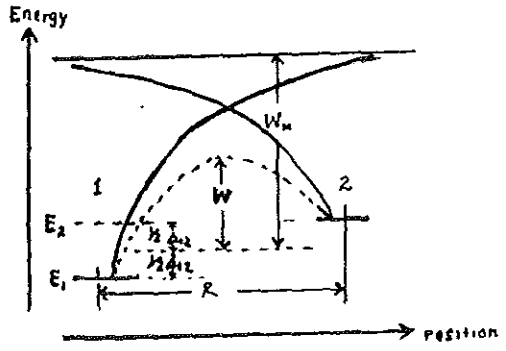

Fig. 2.3 Parameters for a CBH hop between states 1 and 2

The effective relaxation time for this model has the form

$$\tau = \tau_{oh} \exp\left(\frac{W}{KT}\right) \cdot \frac{1}{\cosh(\Delta/2KT)} \qquad (2.11)$$

If one is to work at too low a temperature then, as generally $W>>KT$, an activation energy much greater than the Debye energy is expected and hence imprically τ_{oh} is taken to be of the order of an inverse Debye frequency.

Using Eqns (2.10) and (2.11), we can calculate the a.c. conductivity within the pair approximation to be expected for the CBH model by substitution into Eqn. (2.4). τ is an exponential function of W and, since W and R are related through Eqn(2.10), hence varies rapidly with R. Therefore when from (2.10) the integral over R is transformed to one over τ by making the substitution

$$dR = \frac{KT}{\tau} \frac{1}{dW/dR} d\tau \qquad (2.12)$$

the integral (2.4) gives the real part of the conductivity to be

$$\sigma_i = \frac{\pi}{6} e^2 g_o^2 \omega \int \frac{[R^2(dR/dW)]\omega d\tau}{(1+\omega^2\tau^2)}$$

$$X \iint \frac{dE_i\, dE_2}{\cosh[\beta/2(E_1-E_2)]\{\cosh[\beta/2(E_1+E_2)] + \cosh[\beta/2(E_1-E_2)]} \qquad (2.13)$$

Since the real part of the conductivity is strongly peaked where $\omega\tau \sim 1$, the integral over τ can be approximated [17] by $(\pi/2)\ [R^4(dR/dW)]$ in such a way that this function is evaluated at R_ω, the value of R corresponding to $\omega\tau=1$. Although R_ω is in principle dependent on ε_1 and ε_2 the energy factor in (2.12) restricts the hopping processes to states close to the Fermi level and hence in evaluating R_ω we can use the approximate form of (2.11) with $\Delta \lesssim KT$. R_ω is then given by the solution of the equation

$$W(R_\omega) = -KT\ \ell n(\omega\tau_{oh}) \qquad (2.14)$$

substituting this into Eqn(2.10) we obtain, for a single electron CBH model,

$$R_\omega = \frac{e^2}{\pi\varepsilon\varepsilon_o[W_m + KT\ \ell n(\omega\tau_{oh})]} \qquad (2.15)$$

This equation implies that the hopping distance is a function of both frequency and temperature.

The energy integral of (2.13) shall be evaluated for two cases. In the narrow-band case ($\Delta_o << KT$) we obtain

$$\sigma_1 = \frac{\pi^2}{24} N^2 e^2 \omega\ [R^4 dR/dW]$$

$$= \frac{\pi^3 \varepsilon\varepsilon_o}{24} N^2 \omega R_\omega^6 \qquad (2.16)$$

and in the wide-band case ($\Delta_o >> KT$) we obtain

$$\sigma_1 = \frac{\pi^3 g_o^2}{12} (KT)^2 \omega R_\omega^6 \qquad (2.17)$$

By differentiating the $\ell n\sigma$, in Eqns. (2.5) and (2.16, 2.17), with respect to $\ell n\omega$ at a constant temperature it is straight forward to derive Eqn. (2.8) i.e.,

$$S = 1 - \frac{6KT}{W_m + KT\ell n(\omega\tau_{oh})} \qquad (2.18)$$

Thus in the CBH model the frequency exponent of $\sigma(\omega)$ is predicted to decrease from unity with increasing temperature and decreasing frequency.

2.6 Imaginary Component of the Frequency-Dependent Loss

So far we have considered the real part of the ac loss, σ_1, which leads to the sample resistance. It is also important to study the imaginary component of the ac loss, σ_2, which has a dispersive contribution to the capacitance.

In the simple model we considered the imaginary part of the conductivity, Eqn. (2.4), has the form.

$$\frac{\sigma_2}{\omega} \alpha \int_{\tau_o} F(R) \frac{d\tau}{\tau(1+\omega^2\tau^2)} \qquad (2.19)$$

where the physical details are contained in the function F and

in the relationship between R and τ. The term τ in the denominator here implies a strong contribution to σ_2 from states with short relaxation times in the region of τ_o.

For the CBH model the evaluation of Eqn. (2.19), to a first order approximation (for small KT/W_m), and its equivalent for the real part of the ac loss gives [17, 18] the result

$$\frac{\sigma_2}{\sigma_1} = \frac{-2\ell n(\omega\tau_{oh})}{\pi} \left[1 + \frac{3KT\ \ell n(\omega\tau_{oh})}{W_m}\right] \qquad (2.20)$$

2.7 Interpretation of AC Loss Data for Amorphous Semiconductors.

Most of the ac loss measurements reported for amorphous semiconductors have been of conductance. But what is measured in a given experiment is the total conductance $G_{tot}(\omega)$ of the sample at the particular frequency and temperature. In general, this can be written as

$$G_{tot}(\omega) = G_{ac} + G_{dc} \qquad (2.21)$$

where G_{dc} is the dc conductivity, and it is tacitly assumed that the ac and dc conductivities are due to completely different processes. In separating these two components G_{ac} is taken to be due to hopping between defect centers and G_{dc} due to band conduction in extended states.

conductance data obtained from amorphous semiconducting samples generally follows an ω^s form. Neglecting the frequency dependence of S, the relation $G_{tot}(\omega) - G_{dc} \doteq G_{ac}(\omega) = A\omega^s$ is fitted with G_{dc} as a variable parameter to obtain the best fit using the conductivity data at a given temperature. For the fitting procedure a least-mean-squares-fitting program can be used.

The total measured capacitance $C_{tot}(\omega)$, like conductance is composed of two components.

$$C_{tot}(\omega) = C_{ac} + C_{\infty} \qquad (2.22)$$

These two components arise from different processes, C_∞ being due to high-frequency atomic and dipolar vibrational transitions, whereas C_{ac} is the contribution from the relaxation processes. The usual method of eliminating the nondispersive component is numerical differentiation of the capacitance data. Upon differentiating the capacitance data the constant term involving C_∞ drops out. Thus, if the dispersive part of the capacitance obeys the power law

$$C(\omega) \sim \omega^{s'-1} \qquad (2.23)$$

where S' is not equal to S, the frequency exponent for the real part of the conductivity, a plot of $\log_{10}[-dc/d(\ln\omega)]$ versus $\log_{10}\omega$ should yield a straight line of slope S'-1.

One of the several methods of eliminating the nondispersive component is the adjustment of C_∞ until the resulting $C(\omega)$

obeys a power-law dependence. In this work this method was followed.

It has been shown [17, 18] that the ratio of the imaginary and real ports of the conductivity, related to the frequency-dependent capacitance and conductance by

$$\frac{\sigma_2(\omega)}{\sigma_1(\omega)} = \frac{\omega C(\omega)}{G(\omega)} \qquad (2.24)$$

has a characteristically different functional form for the various mechanisms of dielectric relaxation. For the CBH model, this is expressed in Eqn (2.20). The fit of this ratio is used in determining the difference S'-S which can be used to calculate the frequency exponent S for the conductance. The determination of S on the other hand helps to estimate W_m that indicates the dominant center contributing to the loss at a particular frequency and temperature.

3 EXPERIMENTAL METHOD AND TECHNIQUES

3.1 Sample Preparation

The hydrogenated amorphous silicon films, studied in this work are prepared by the method known as Homo Chemical Vapour deposition (CVD). We have two series of samples. These are series of samples that are prepared under dark condition and samples that are prepared under Ultra-violet light illumination.

In both the dark and UV-series there are samples that are prepared on sodium glass (N_a) and that are prepared on corning glass (CG 7059) substrates. Table 1 represents a data of photometric measurements and technological parameters.

TABLE 1

Sample	T_s (°C)	d(cm)	ℓ(cm)	b(cm)	n	Eq(eV)
D-1-C	358	1.35×10^{-4}	.480	.068	3.80	1.59
D-1-Na	358	1.35×10^{-4}	.460	.075	3.80	1.59
D-2-C	279	1.63×10^{-4}	.474	.072	3.58	1.67
D-2-Na	279	1.63×10^{-4}	.408	.058	3.58	1.67
D-3-C	235	1.68×10^{-4}	.462	.072	3.39	1.71
D-3-Na	235	1.68×10^{-4}	.464	.064	3.39	1.71
UV-1-C	361	1.26×10^{-4}	.530	.066	3.55	1.60
UV-1-Na	361	1.26×10^{-4}	.438	.064	3.55	1.60
UV-2-C	281	1.64×10^{-4}	.464	.056	3.68	1.66
UV-2-Na	281	1.64×10^{-4}	.472	.076	3.68	1.66

The parameters in Table 1 above are

T_s substrate temperature

d thickness of the film

ℓ length of the film

b contact separation

n index of refraction

E_g optical gap

The dimensions d,ℓ, and b are shown in figure 3.1 below.

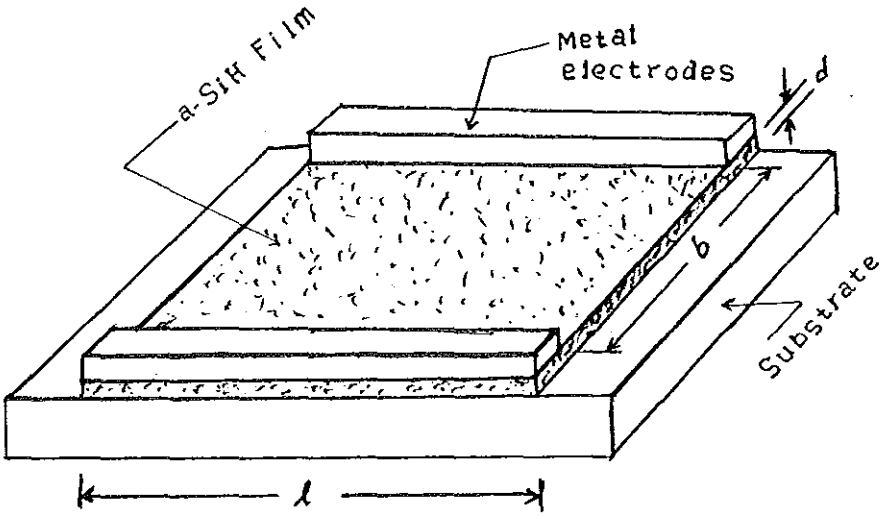

Fig. 3.0 Sample geometry

3.2 Features of Measuring Instruments

3.2.1 PA-Meter/DC Voltage Source

The HP-Model 4140B pA Meter/DC Voltage source comprises a high stability pA Meter with 10^{-15}A (max) resolution coupled with two programmable DC voltage sources (V_A and V_B). The PA meter has an accuracy of 0.5% over wide measurement ranges ($\pm$ 0.001x 10^{-12}A ~ $\pm$ 1.999x10^{-2}A) enabling stable pA current measurement at 10^{-15}A.

One of the two programmable DC voltage sources (V_A) can operate not only as a programmable DC voltage source, but also as a unique stair case and accurate ramp generator. The DC voltage source has an output range of $\pm$100V or $\pm$10V. The ramp wave generated by the DC voltage source has a step voltage from -10.00V to +10.00V and a ramp rate from 0.001V/S to 1.000V/S.

The HP-Model 4140B can be set to measure current as a universal pA meter and has an ability of accurate I-V/C-V measurements. Its zero offset current capability cancels leakage current of test leads and fixtures for accurate current measurements. It also provides HP-IB for remote control and data output Via the HP-IB.

3.2.2 Digital Multimeter (DMM)

The HP Model 3478A Digital Multimeter (DMM) is able to measure voltage and current, both AC and DC, and also resistance. It is a fully programmable HP-IB digital multimeter.

The DMM has five ranges of DC volts, 30mV, 300mV,3V,30V and 300V. In this work it is used to measure the volt corresponding to the thermocouple which is used to measure the temperature of the sample. In all the three types of measurements done in this work there was a need for temperature measurement and thus the meter was remotely controlled Via HP-IB by using a program constructed of remote command codes of its functions.

3.2.3 Multifrequency LCR Meter

The other main unit of measurement used in this work was the HP Model 4275A Multifrequency LCR Meter. This meter is an instrument designed to measure the various component parameter values of impedance elements in the relatively high frequency range. It measures inductance, capacitance, resistance, dissipation factor, quality factor, conductance, suceptance, reactance, impedance and phase angle.

A total of 10 test signal frequencies which have a frequency accuracy of 0.01% are available in the HP Model 4275A Multifrequency LCR Meter. The test frequencies are selected in a 1-2-4-10 sequence from 10KHZ to 10MHZ by the frequency STEP control. An a.c. signal, with amplitude range of 1mV to 1V, can be set to the sample with a help of an oscillation level control button. This meter has a zero offset compensator which can be used to perform proper compensation for cancelling stray capacitance, residual inductance, conductance, and resistance of test fixture and leads used in the circuit. In this work the LCR meter is used in a.c. loss measurement to measure conductance and capacitance.

3.3 Experimental Procedures and Results

The main aim of this work is to investigate the electrical conductivity of a-si:H films, prepared by HOMO CVD method, and thus to determine some physical parameters characterizing the material.

Three kinds of measurements have been performed in this work these are current-voltage characteristics, temperature dependence of conductivity and ac loss measurements.

3.3.1 Preliminaries

Before going into detail of the main experiment it was necessary to prepare appropriate environmental conditions. After preparing a good insulator substrate for the sample, contacts are constructed on the substrate in such a way that it is possible to install and remove the sample easily. The next step to this was the construction of a heater. The heater used in this work was constructed by uniformly winding a high resistive conductor on a glass tube. Figure 3.1 is the schematic representation of the heater used in this work. Thus putting the sample inside the tube the temperature of the sample can be varied as required.

For measuring the temperature of the sample a Chromel-Alumel thermocouple was constructed in our laboratory. For the calibration of the thermocouple a reference table [28] for the

corresponding thermocouple was used and comparision between the table and the reading was done for temperature range between the melting point of ice and the boiling point of water, using a mercury thermometer attached to the thermocouple.

In addition to the construction of thermocouple a program was constructed (Appendix A) that can be used to display the temperature and plot its variation with time, on the computer screen. This helps in stabilization of temperature and in taking the corresponding temperature of any data by remotely controlling the digital Multimeter that reads the voltage in the thermocouple.

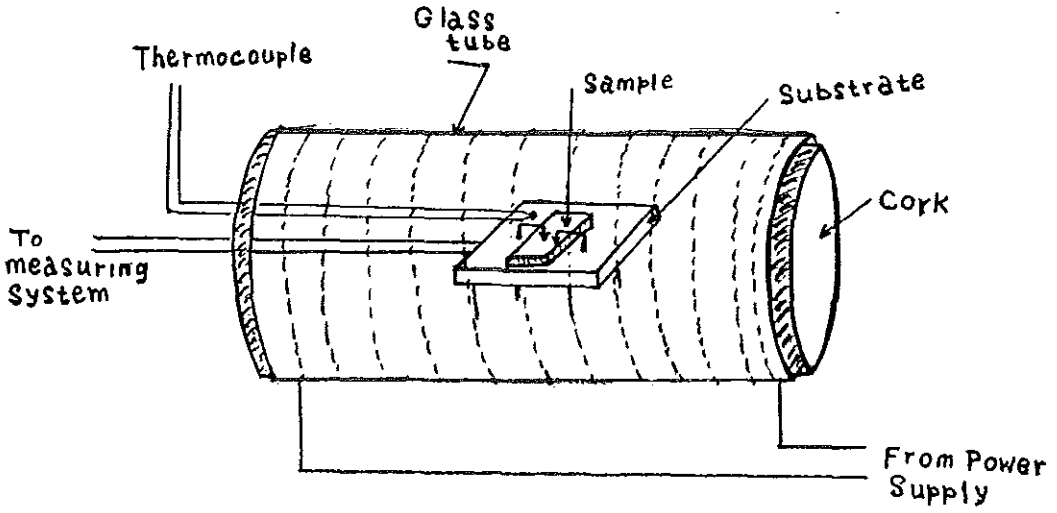

Fig. 3.1 Schematic representation of the heater containing the sample under investigation.

In the construction of the program that converts the thermocouple volts into the corresponding temperature the polynomial used was

$$T = A_0 + A_1 V + A_2 V^2 + A_3 V^3$$

where A_0, A_1 , A_2 and A_3 are constant coefficients to be determined and V the voltage from the thermocouple. In determining the coefficients the Chebyschev polynomial from the numerical analysis software library was used. The values used for the voltage V, in determining the coefficients, are those from the reference table for Chromel-Alumel thermocouple.

3.3.2 I-V Characteristics Measurement

In the I-V characteristics measurement three voltage ranges were choosen. These are -1V to 1V, -10V to 10V and -100V to 100V ranges. The voltage source used for this measurement is the programmable DC voltage source V_A of the HP-Model 4140B pA Meter / DC voltage source. The mode of voltage used in all the three ranges is ramp wave. Ramp rates of 0.005V/S, 0.05V/S, and 0.5V/S, respectively, are used for the choosen ranges of measurement.

The experimental set up for the I-V characteristics measurement is shown in Figure 3.2 without the Isolated DAC/power supply programmer. The stability of the temperature choosen for mea-

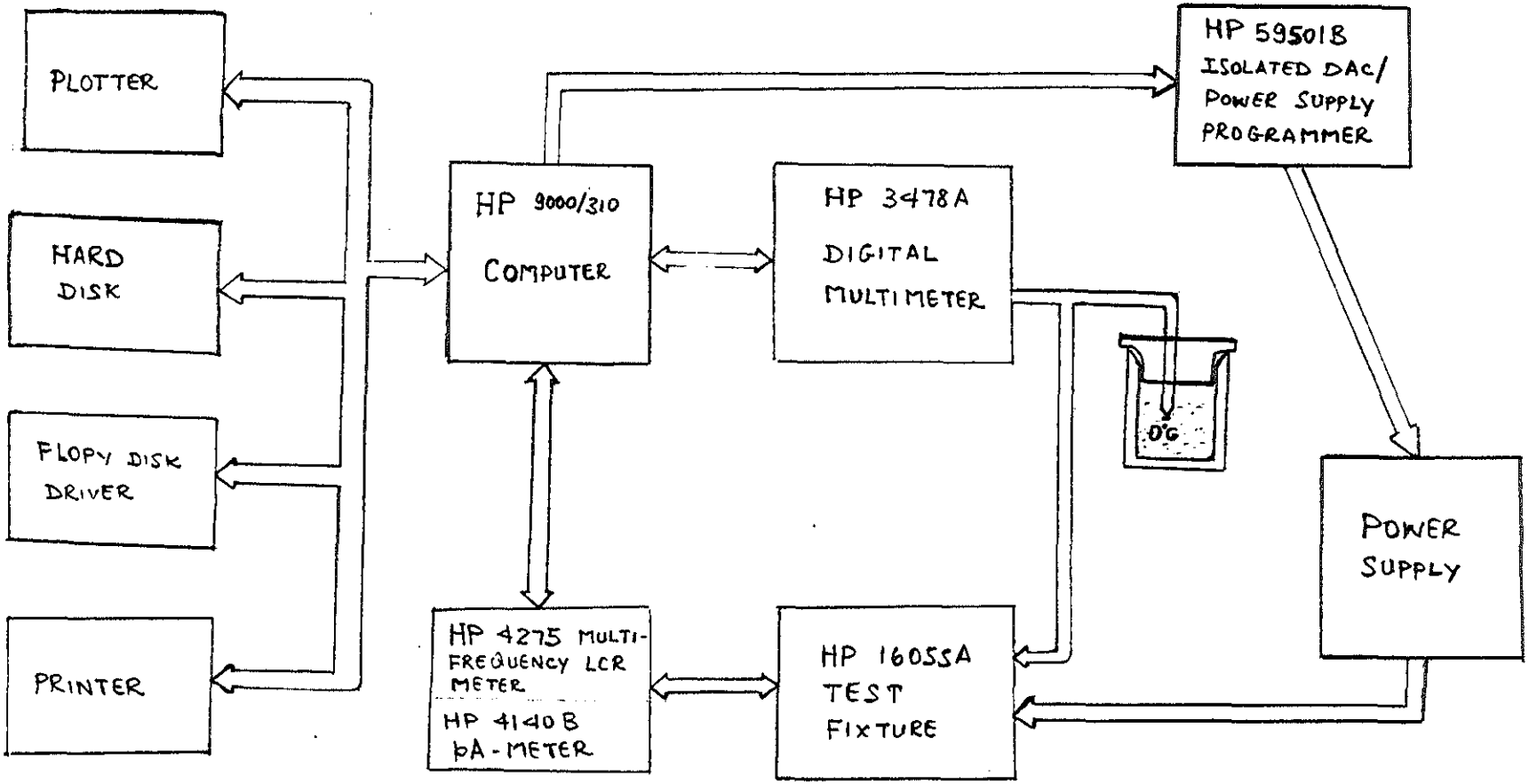

Fig.3.2 Experimental Set up

surement was constantly controlled by adjusting the power supply manually. Eight temperature ranges were choosen, for each voltage range, in order to observe the effect of temperature on the I-V characteristics.

For the -1V to 1V range a voltage step of 0.02V was used and this allows the possibility of observing the I-V characteristics even within a range of -0.1V to 0.1V. The results for this range of measurement are presented in Fig.(3.4) and (3.5). Figure 3.4 shows the I-V characteristics for two different samples (UV2C and D1C) that are prepared with different conditions but with the same substrate and measured at the same temperature and one of them (i.e., UV2C) measured at two temperatures. Figure 3.5 shows the current voltage characteristics for two samples (UV2Na and UV2C) prepared in the same condition but with different substrates and measured at different temperatures.

All the steps, in the -1V to 1V range of measurement, are repeated for the -10V to 10V and the -100V to 100V ranges except that a voltage step of 0.2V and 2V, respectively, are used in these ranges. Figure 3.6 represents the I-V characteristics for sample UV2Na at two temperatures (338K, and 373K) for the -10V to 10V range of measurement.

Figures 3.7 and 3.8, respectively represent the I-V characteristics for sample UV1C, at three different temperatures (295K, 323K, and 417K), and for sample UV1Na, at three temperatures (295K, 323K, and 355K) in the range -100V to 100V. Figure 3.9 represents the I-V characteristics for sample UV1Na at T=307K and D1Na at T= 297K.

3.3.3 σ-T Measurement

The experimental set up used for temperature dependent conductivity measurement is shown in Fig. 3.2. In this measurement room temperature up to 414K was used. In investigating the temperature dependence of conductivity there is a need for a continous change in temperature. The rate of change of temperature should also be constant i.e., the temperature should increase linearly during all the time of measurement in the range choosen. But the temperature obtained as a result of a uniformly increasing applied voltage was observed to change in a power law.

The problem of getting a temperature that is linearly changing with time was solved by the use of a circuit that consist of the Isolated DAC/Power Supply programmer and a current amplifier circuit. After finding the law of change of temperature as a result of a uniformly increasing voltage a program was constructed in such a way that a voltage that varies in a certain law and gives a temperature that is linearly increasing, will be output with the help of the Isolated DAC/Power Supply Programmer. Since the maximum output of the programmer is 10mA the current amplifier was used in order to get the required amount of current to the heater. The circuit diagram used for obtaining a linearly increasing temperature from the heater is shown in fig. 3.3.

In the σ-T measurement the bias voltage used are 1V and 10V. The program used in this measurement was given in Appendix C. For all the samples investigated the same temperature dependence of conductivity was obtained. Figure 3.10 shows the plot of conductivity versus reciprocal temperature for samples D1C D2C, and D3C.

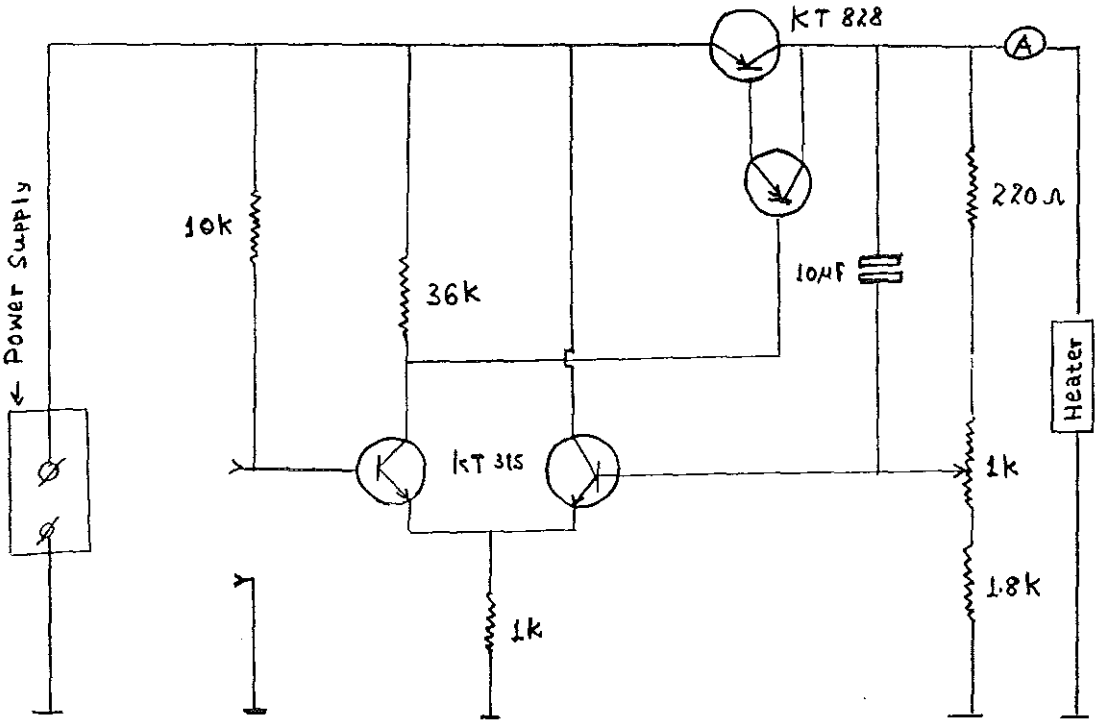

Fig. 3.3 Schematic representation of the circuit used to get a near linearly increasing temperature from the heater.

3.3.4 AC Measurement

In the frequency dependent loss measurement the same set up as for the I-V measurement was used except that in this case the pA Meter is replaced by the Multifrequency LCR Meter. The quantities measured were capacitance and conductance. In the

measurement at a particular temperature the initial step was to make the zero-offset so as to avoid the contribution from leads in the circuit and the substrate. The frequency range used in this experiment is from 10KHZ to 1MHZ. The program in Appendix A was used to control the stability of temperature. Four temperature points are randomly choosen.

Fig. (3.12) and (3.13), respectively, represent the capacitance versus angular frequency and conductance versus angular frequency plots for sample UV1Na investigated at 443K. It is clear that both quantities, i.e., capacitance and conductance, vary in a power law of the angular frequency of the applied field.

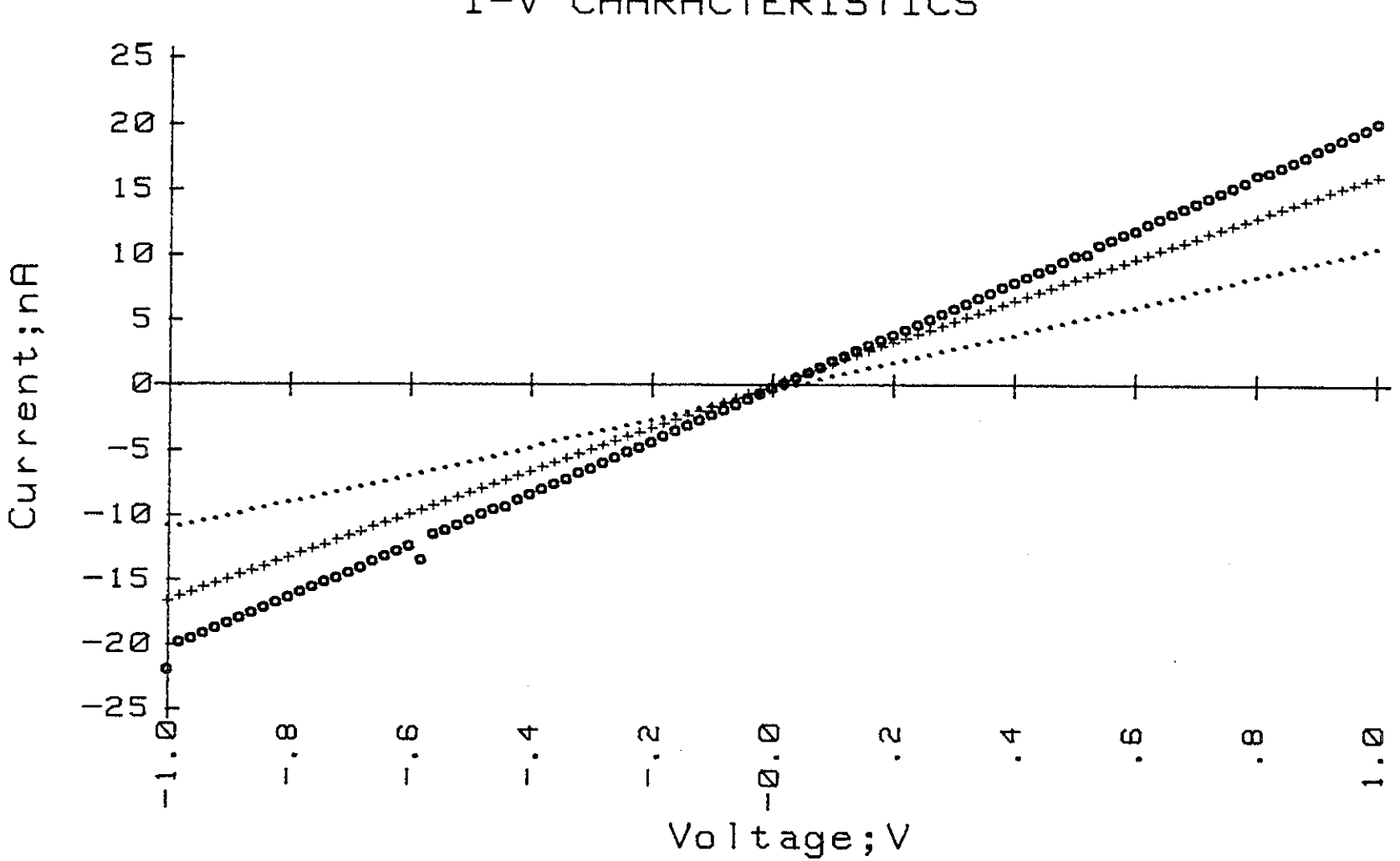

Fig. 3.4 . UV2C, T=417K; + D1C, T=417K; o UV26, $Ix10^{3}$, T=323K

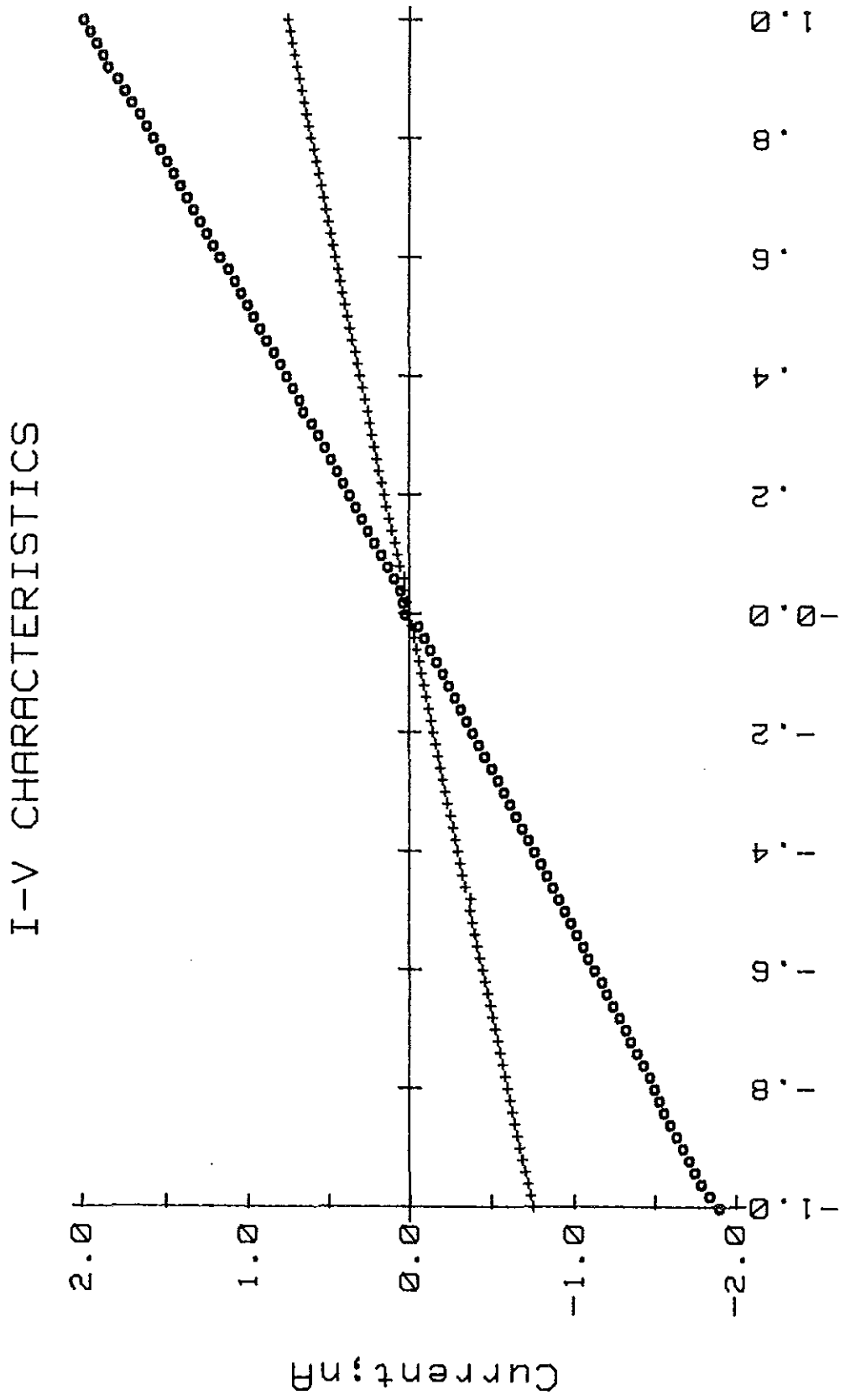

Fig.3.5 + UY2C, T=373K; o UY2Na, Ix10, T=323K

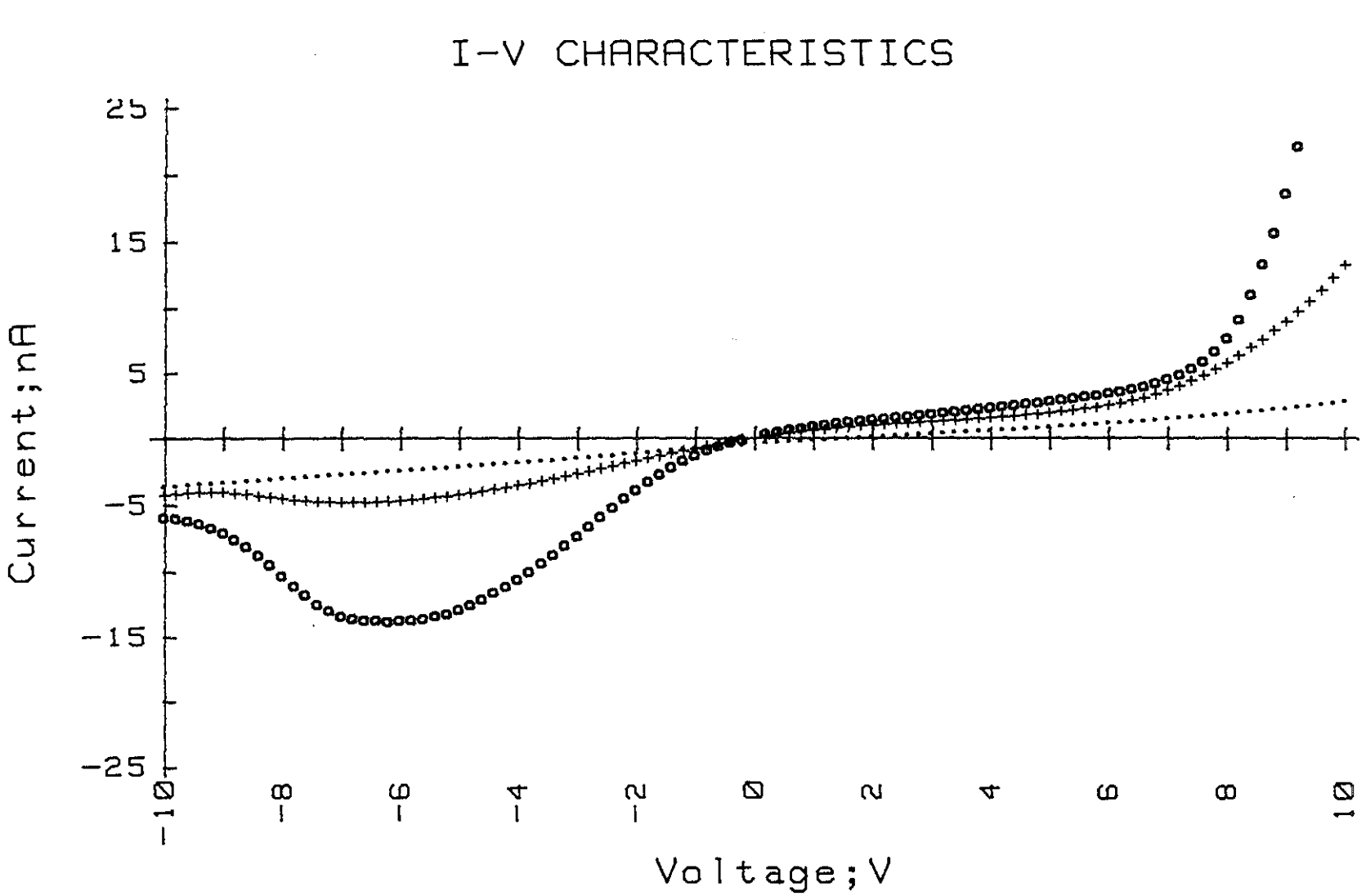

Fig.3.6 o UV2Na, T=373K; + UV2Na, T=355K; . UV2Na, T=338K

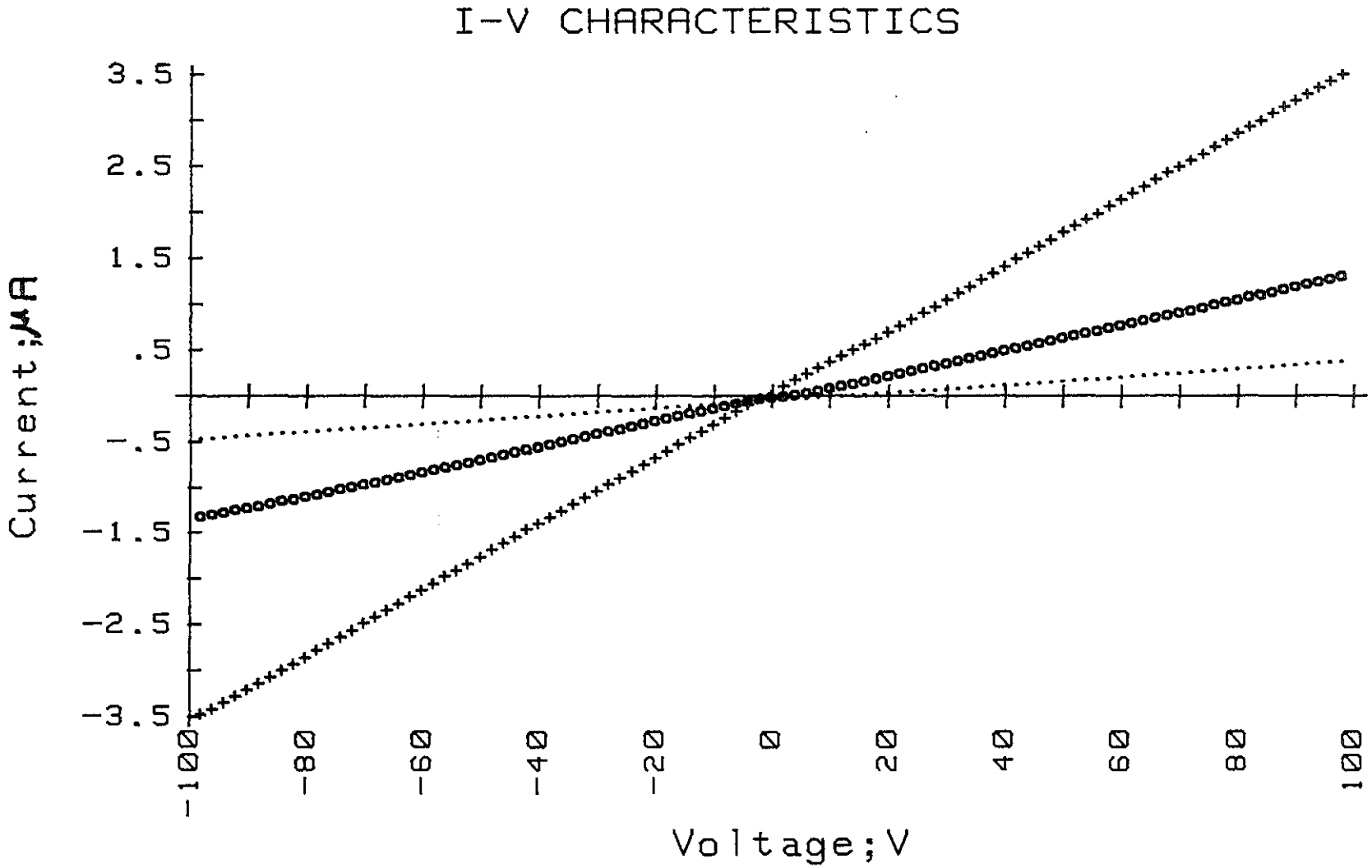

Fig.3.7 . UV1C, Ix10^3, T=295K; o UV1C, T=417K; + UV1C, Ix10^3, T=323K

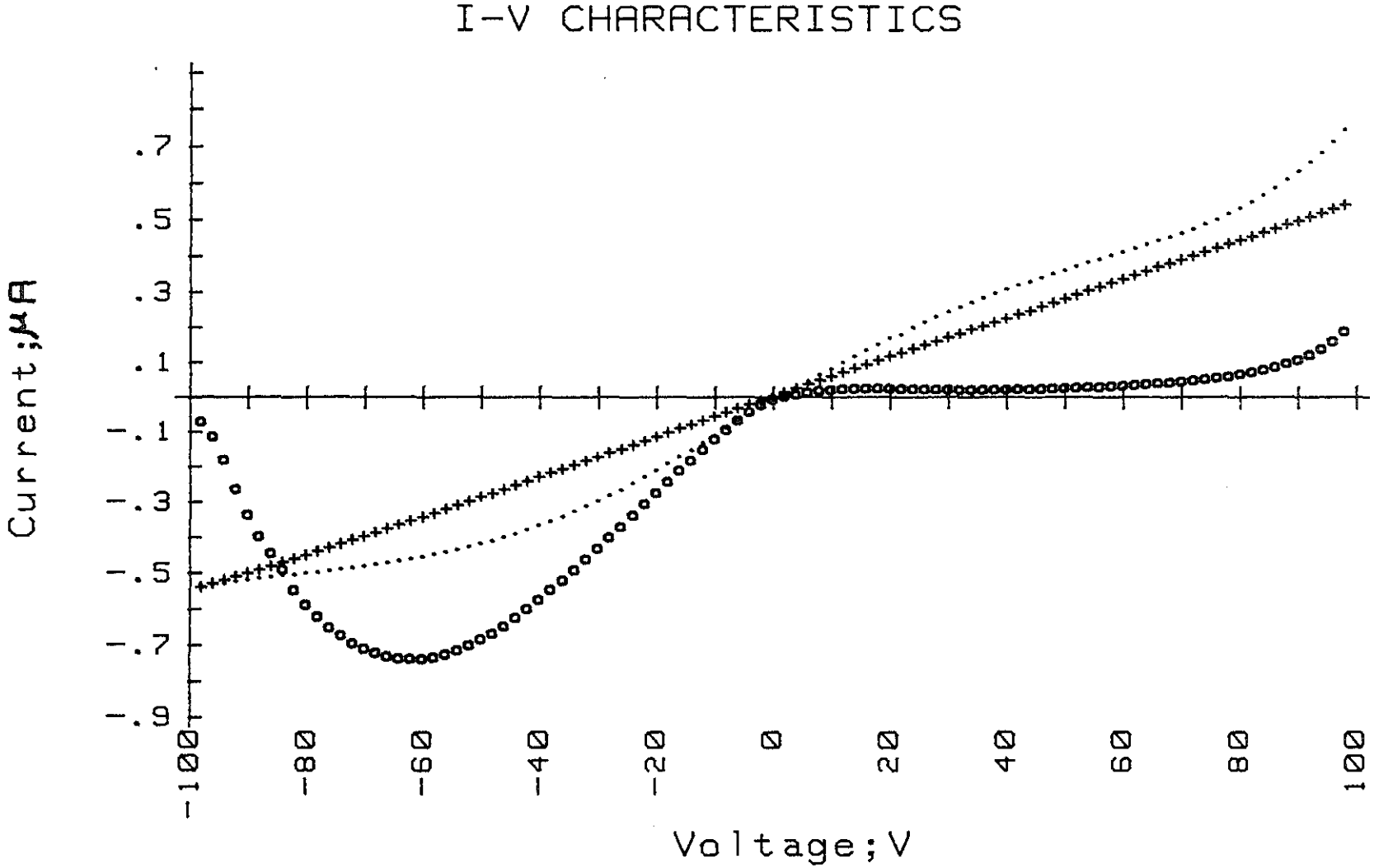

Fig. 3.8 o UVlNa, T=355K; + UVlNa, Ix10^3, T=295K; . UVlNa, T=323K

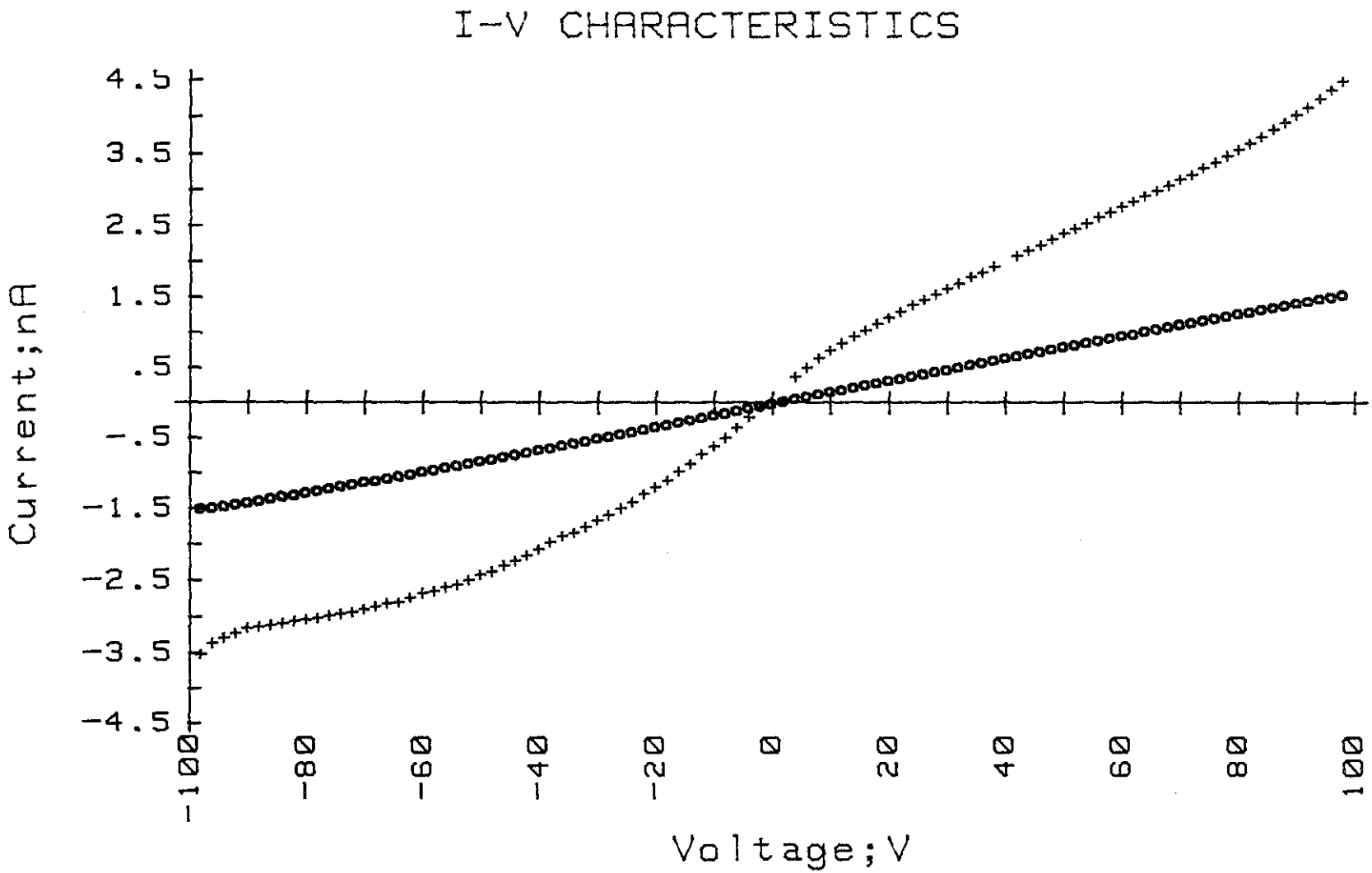

Fig. 3.9 o UV1Na, T=307K; + D1Na, T=297K

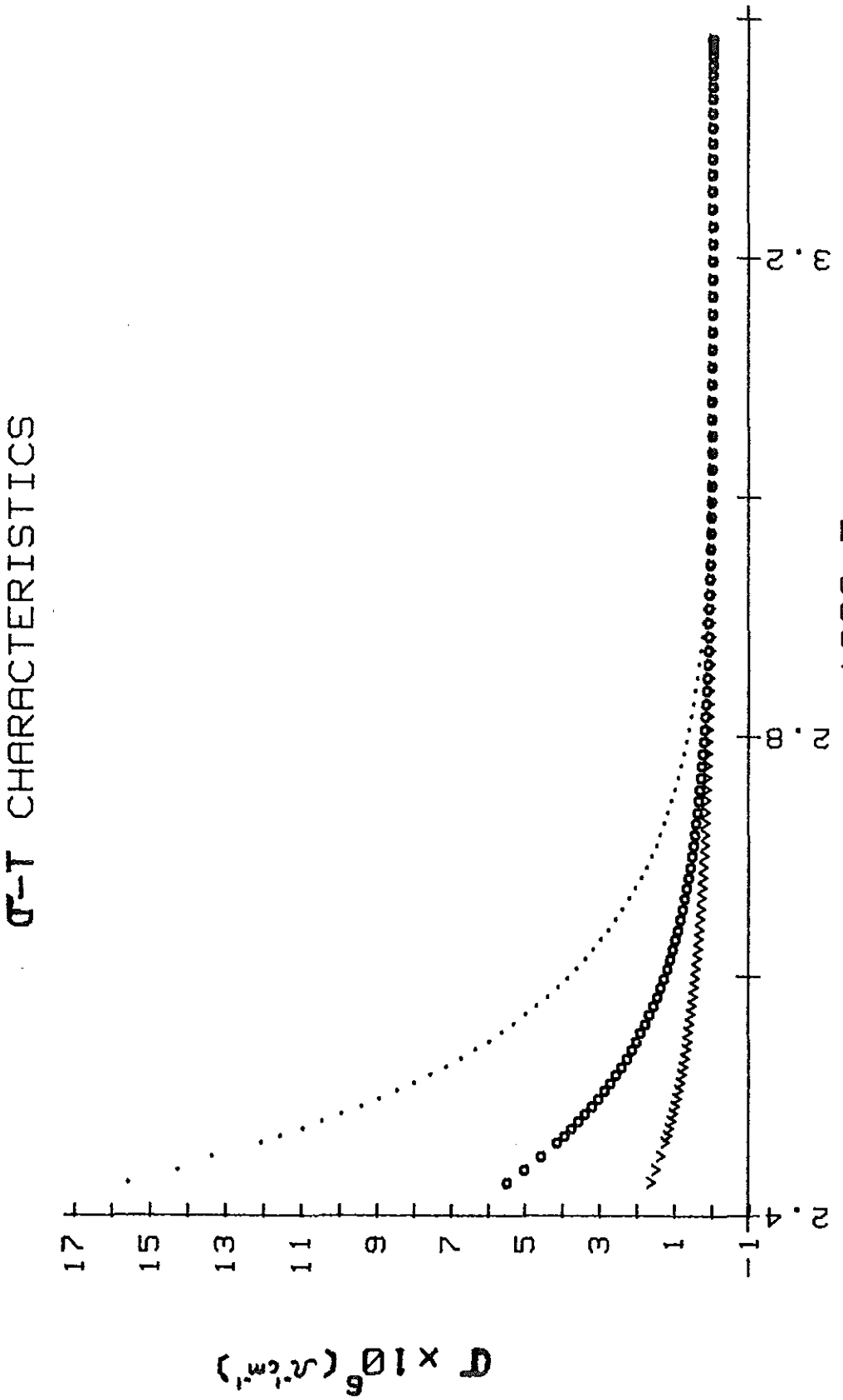

Fig. 3.10 . D1C; o D2C; v D3C

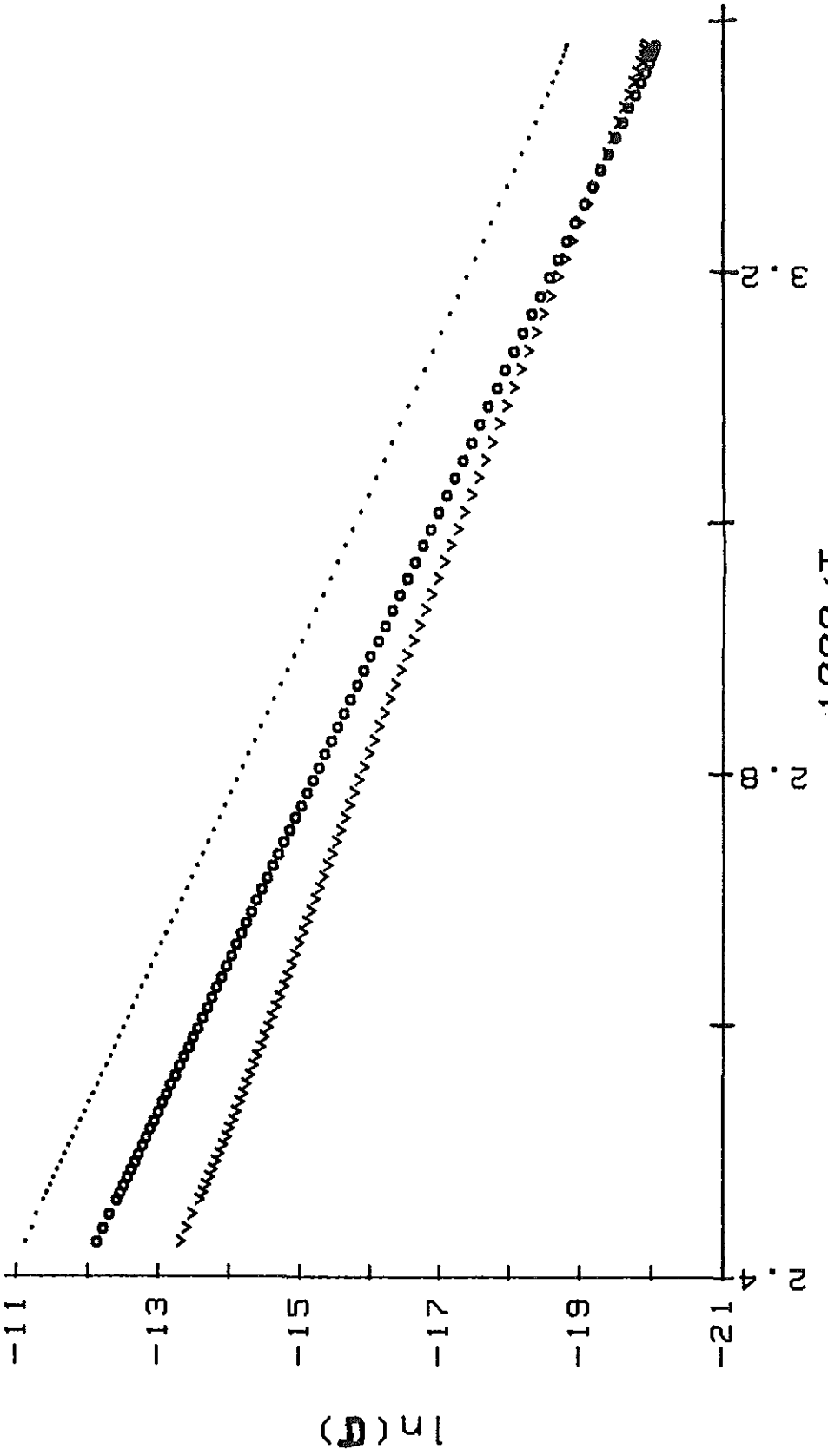

Fig. 3.11 . D1C; o D2C; y D3C

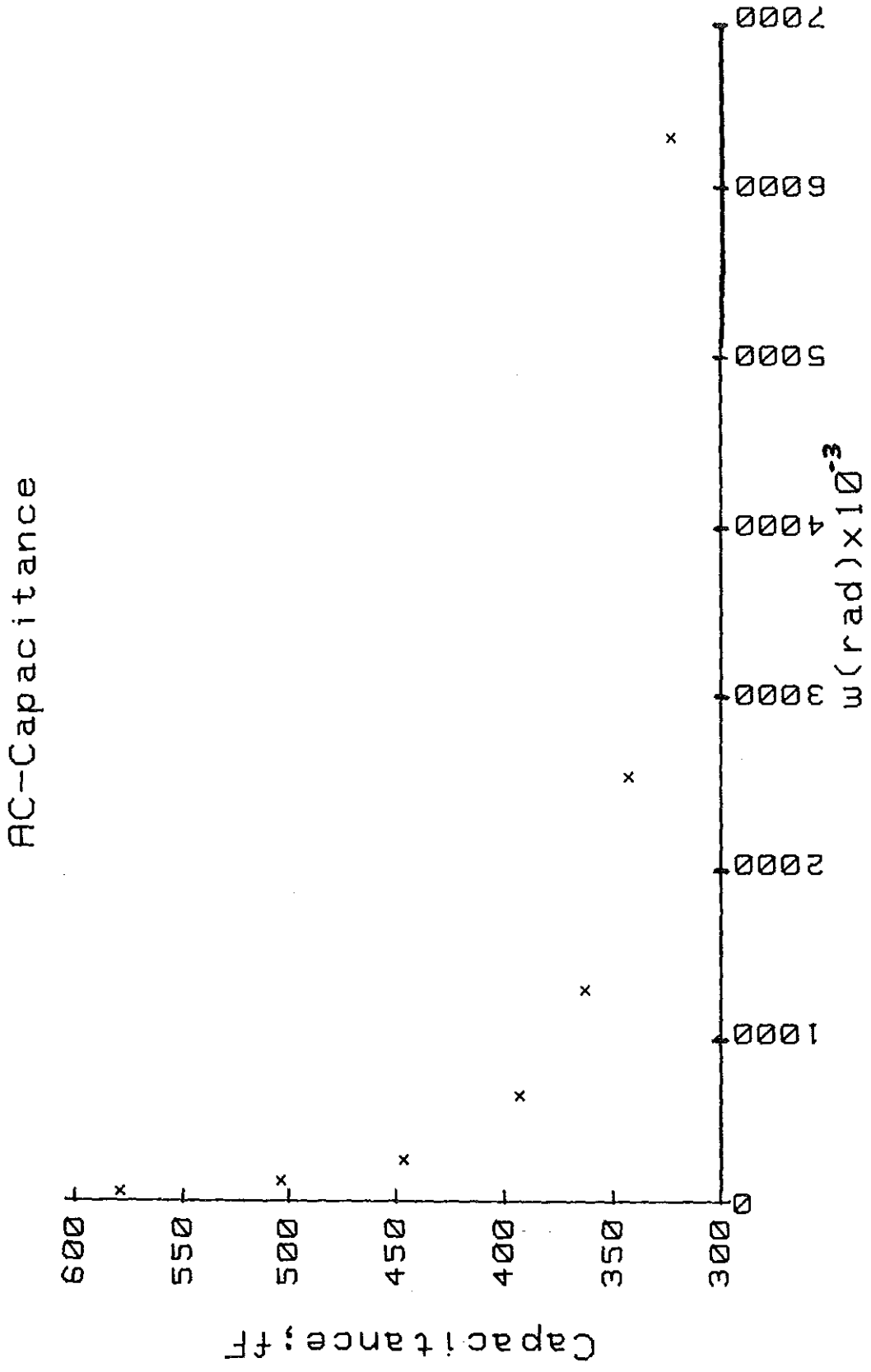
AC-Capacitance
Capacitance;fF
600
550
500
450
400
350
300
0
1000
2000
3000
4000
5000
6000
7000
w(rad)x10^-3

Fig. 3.12

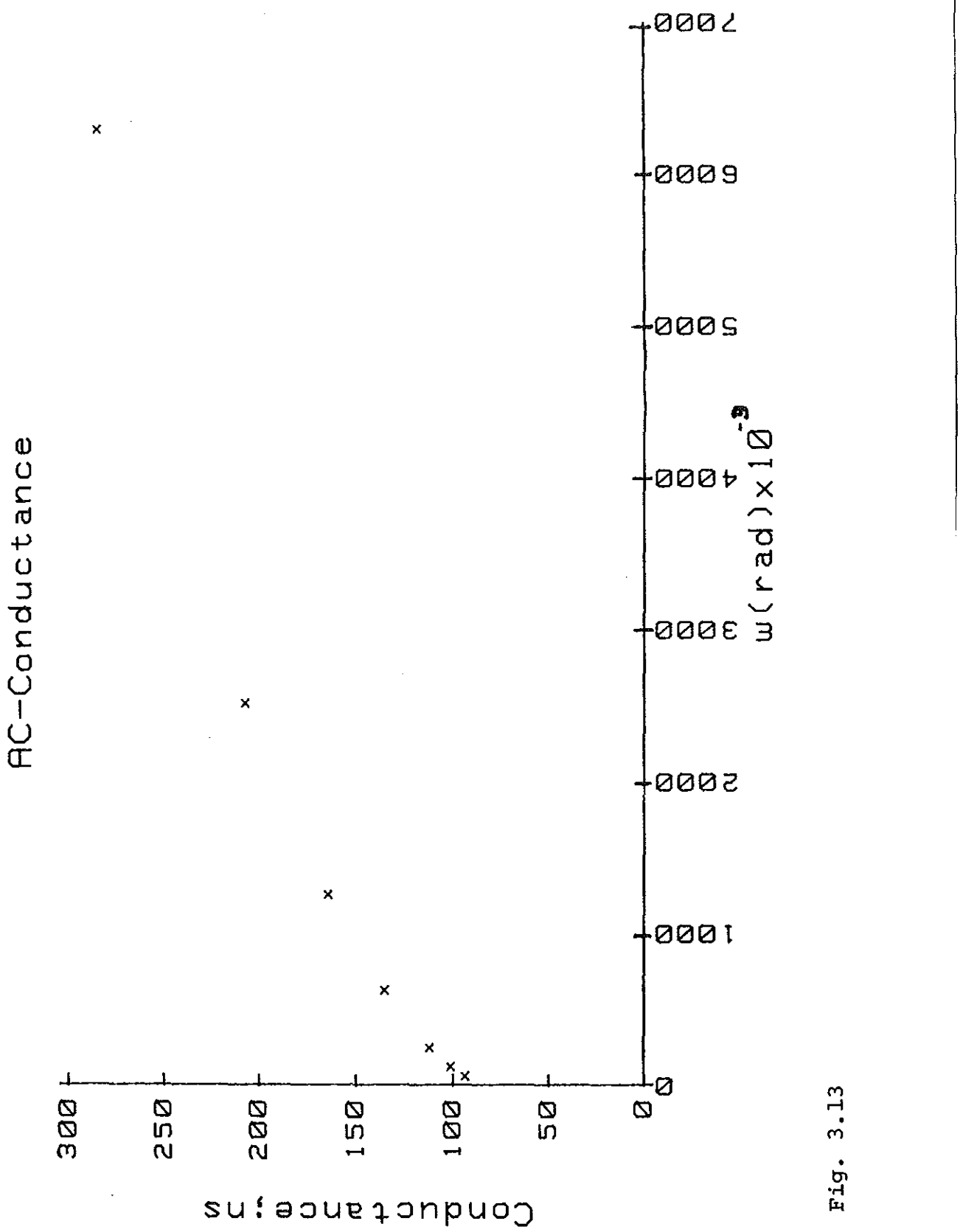
AC-Conductance
Conductance;ns
300
250
200
150
100
50
0
0
1000
2000
3000
4000
5000
6000
7000
ω(rad)x10⁻⁶

Fig. 3.13

4. DISCUSSION OF RESULTS

As shown in figures (3.4) and (3.5) the I-V characteristics for the -1V to 1V range of measurement exhibits a linear behavior at all temperatures for all the samples investigated. But since we have samples that are prepared with two types of substrates, under dark and ultraviolet illumination, with three different substrate temperatures and with different thicknesses, the result shows that for this range of measurement the I-V characteristics is independent of all these factors. The linear I-V characteristics implies that we have an ohmic contact. This can be due to the very large contact separation which can give the masking of the contact effect by the bulk sample.

Unlike for the -1V to 1V range of measurement the I-V characteristics for the -10V to 10V, and -100V to 100V range of measurement was found to be linear only for some of the samples in the whole range of temperature. Samples that are prepared with corning glass substrate exhibit a linear characteristics whereas samples that are prepared with sodium glass substrate exhibit a non-linear I-V characteristics. These characteristics are shown in Fig. (3.6), and (3.8) for samples with sodium glass substrate and Fig.(3.7) for samples with corning glass substrate.

The unusal I-V characteristics was observed to be dependent of the temperature. Fig.(3.6) and (3.8) show that the I-V characteristics gets non-linear with increasing temperature. On the other hand Fig. (3.9) shows that the non-linear behavior will

be exhibited at a lower temperature for the samples prepared in dark condition compared to the samples prepared under ultraviolet illumination. Since the study of I-V characteristics is not the aim of this work it is not important to get into detail of the discussion of the I-V characteristics.

Measurement of the temperature dependence of conductivity gives important information. It helps to determine the transport mechanism in the given range of temperature and thus helps to determine some physical parameters that characterizes the material.

In order to see how conductivity depends on temperature and thus on reciprocal temperature the Scattergram plot of the statistical software library was used. The conductivity measured for all the samples in this work shows an exponential dependence to the reciprocal temperature which is consistent with the band conduction model expressed as

$$\sigma = \sigma_0 \exp\left[\frac{-\Delta E}{KT}\right]$$

Figure 3.10 is an example of the reciprocal temperature dependence of conductivity obtained in this work. The figure represents the conductivity of samples D-1-C, D-2-C and D-3-C. Though all the samples show the same dependence on temperature there is a difference in the magnitude of the conductivity for all the three. This implies a difference in the activation energy and the pre-exponential term. In order to estimate the

TABLE 2

Sample	Substrate Temperature ($T^{o}C$)	Thickness d (cm)	Optical gap (eV)	2(ΔE)	Pre-exponential term σ_o (Ω^{-1} m^{-1})
D-1-C	358	1.35×10^{-4}	1.59	$1.492 \pm .003$	$(7.6 \pm .4) \times 10^{3}$
D-2-C	279	1.63×10^{-4}	1.67	$1.32 \pm .03$	$(1.8 \pm .8) \times 10^{3}$
D-3-C	235	1.68×10^{-4}	1.71	$1.222 \pm .006$	$(4.9 \pm .4) \times 10^{1}$
D-1-Na	358	1.35×10^{-4}	1.59	$1.414 \pm .002$	$(5.7 \pm .1) \times 10^{3}$
D-2-Na	279	1.63×10^{-4}	1.67	$1.482 \pm .009$	$(4.6 \pm .6) \times 10^{3}$
D-3-Na	235	1.68×10^{-4}	1.71	$1.54 \pm .03$	$(4.0 \pm .9) \times 10^{3}$
UV-1-C	361	1.26×10^{-4}	1.60	$1.49 \pm .02$	$(5.7 \pm .7) \times 10^{3}$
UV-2-C	281	1.64×10^{-4}	1.66	$1.47 \pm .03$	$(5.1 \pm .5) \times 10^{3}$
UV-1-Na	361	1.26×10^{-4}	1.60	$1.354 \pm .004$	$(3.1 \pm .1) \times 10^{3}$
UV-2-Na	281	1.64×10^{-4}	1.66	$1.660 \pm .005$	$(1.5 \pm .1) \times 10^{2}$

Description: D-dark, UV-Utraviolet, C-corning, Na-Sodium, ΔE-activation energy

activation energy and the pre-exponential term the standard non-linear regression model, of the statistical software library, was used to fit the conductivity versus reciprocal temperature curve. The same result was obtained by using a linear regression software to fit the plot of $\ell n(\sigma)$ versus reciprocal temperature. Figure 3.11 shows the $\ell n(\sigma)$ versus $1000/T$ plot for samples D-1-C, D-2,C and D-3-C. The activation energy determined in this way for all samples is summarized in table 2.

As can be observed from table 2, for all the samples we have, an activation energy that is less than the optical gap. The activation energy for both dark and ultraviolet series samples prepared with corning glass substrate, determined in this work is found to decrease with increasing thickness and decreasing substrate temperature. The activation energy, for both dark and UV-series films prepared with sodium glass substrate is found to increase with increasing thickness and decreasing substrate temperature. But the reason for this behavior of the activation energy is not clear and it needs a more detail study.

Concerning the pre-exponential term we have the reverse of what was obtained for the activation energy, for sodium substrate films. They have a decreasing pre-exponential term with increasing thickness and decreasing substrate temperature. But the corning glass substrate films show to have an increasing pre-exponential term with increasing thickness and decreasing substrate temperature.

Table 3 represents ac loss data for sample UVlNa at four different measurement temperatures. As it is obvious from the table the conductance at a particular frequency is markedly temperature dependent. It is also obvious, from Fig. (3.12) and (3.13), that the ac capacitance and conductance are non-linear functions of the angular frequency, as was expressed by Eqn. (2.23) and (2.5) i.e.,

$$Cac = A\omega^{S'-1} = Ctot - C_{\infty}$$

and

$$Gac = B\omega^{S} = Gtot - Gdc$$

In obtaining the ac capacitance from the total (measured) capacitance the method of fitting $Ctot-C_{\infty}$ to the relation $Cac=A\omega^{S'1}$, with C_{∞} as a variable parameter to obtain the best fit, was used. For the fitting procedure the standard non-linear regression software was used. Figure (4.1) shows the fitting of the capacitance data, of sample UVlNa at 443K, for four different values of C_{∞}. In Fig (4.2) a residual plot was given for the best fit in Fig.(4.1). The same procedure, as for the capacitance, was followed for determining the ac conductance. This is shown in Fig. (4.3).

TABLE 3

f(kHZ)→	10	20	40	100	200	400	1000
T=296;G	.40	.65	1.18	2.66	4.38	6.88	-
C	14	11	9	6	5	4	-
T=317;G	.51	192	1.84	3.77	5.07	13.77	-
C	18	15	12	8	7	5	-
T=392;G	5.90	8.20	11.70	19.10	33.50	44.50	-
C	91	68	50	33	19	16	-
T=443;G	17.2	24.8	35.8	58.8	82.0	131.0	209.0
C	300	224	167	114	84	64	46

G= Conductance(nS); C=Capacitance(f^F); T in kelvin

The fitting method in obtaining the ac components of capacitance and conductance is on the assumption that the frequency exponents S' and S are constant in the frequency range used. Fig. (4.4) and (4.5), respectively, represent the LOG-LOG plots of capacitance versus angular frequency and conductance versus angular frequency. In Fig. (4.4) we have the plot for capacitance without subtraction and with subtraction of C_∞. In Fig. (4.5) we have the plot for conductance without subtraction and with subtraction of Gdc. These plots of capacitance and conductance with subtraction of frequency independent parts are straight lines of slope $S'-1$ and S respectively.

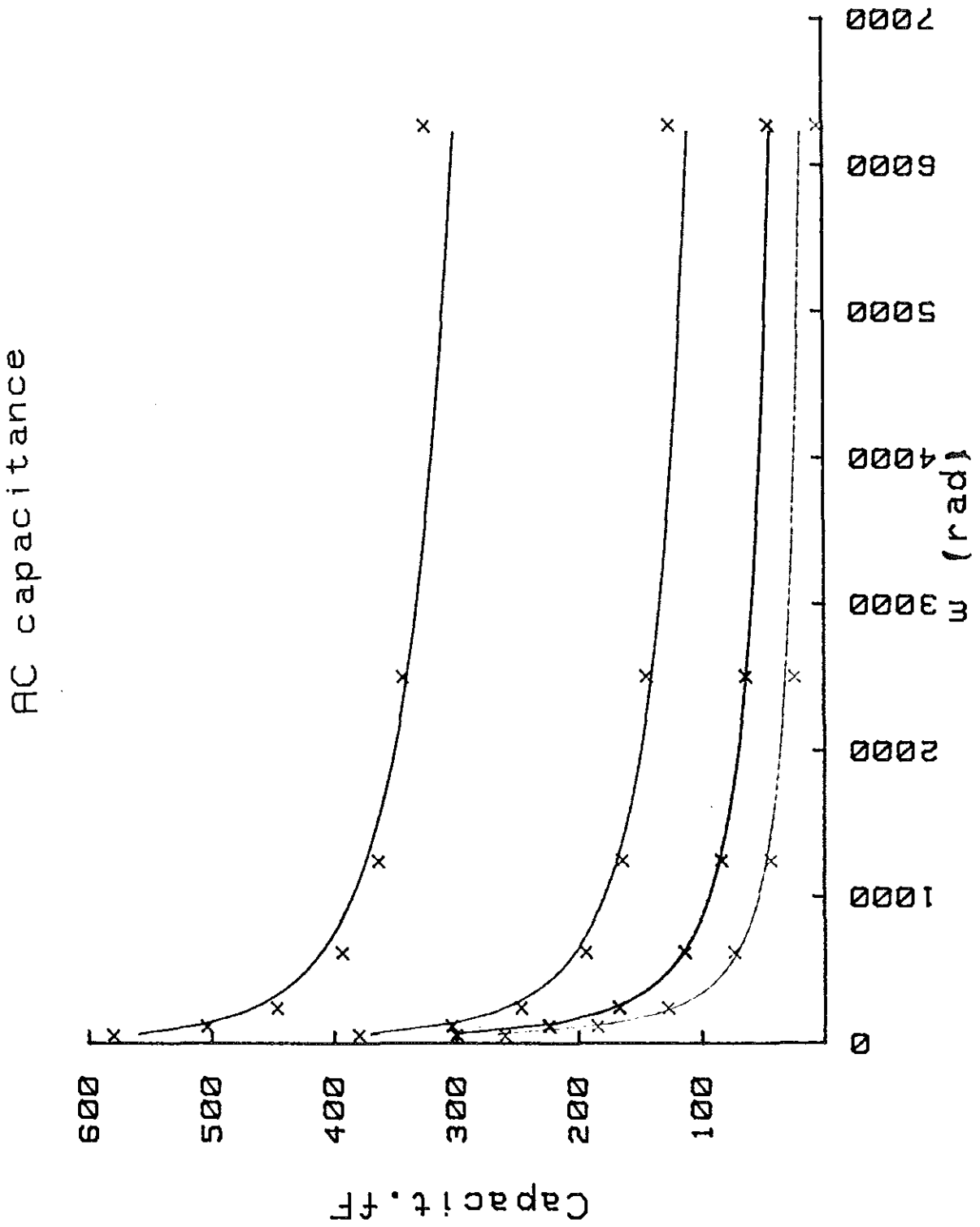
AC capacitance
Capacit.fF
600
500
400
300
200
100
0
1000
2000
3000
4000
5000
6000
7000
ω (rad)

Fig. 4.1

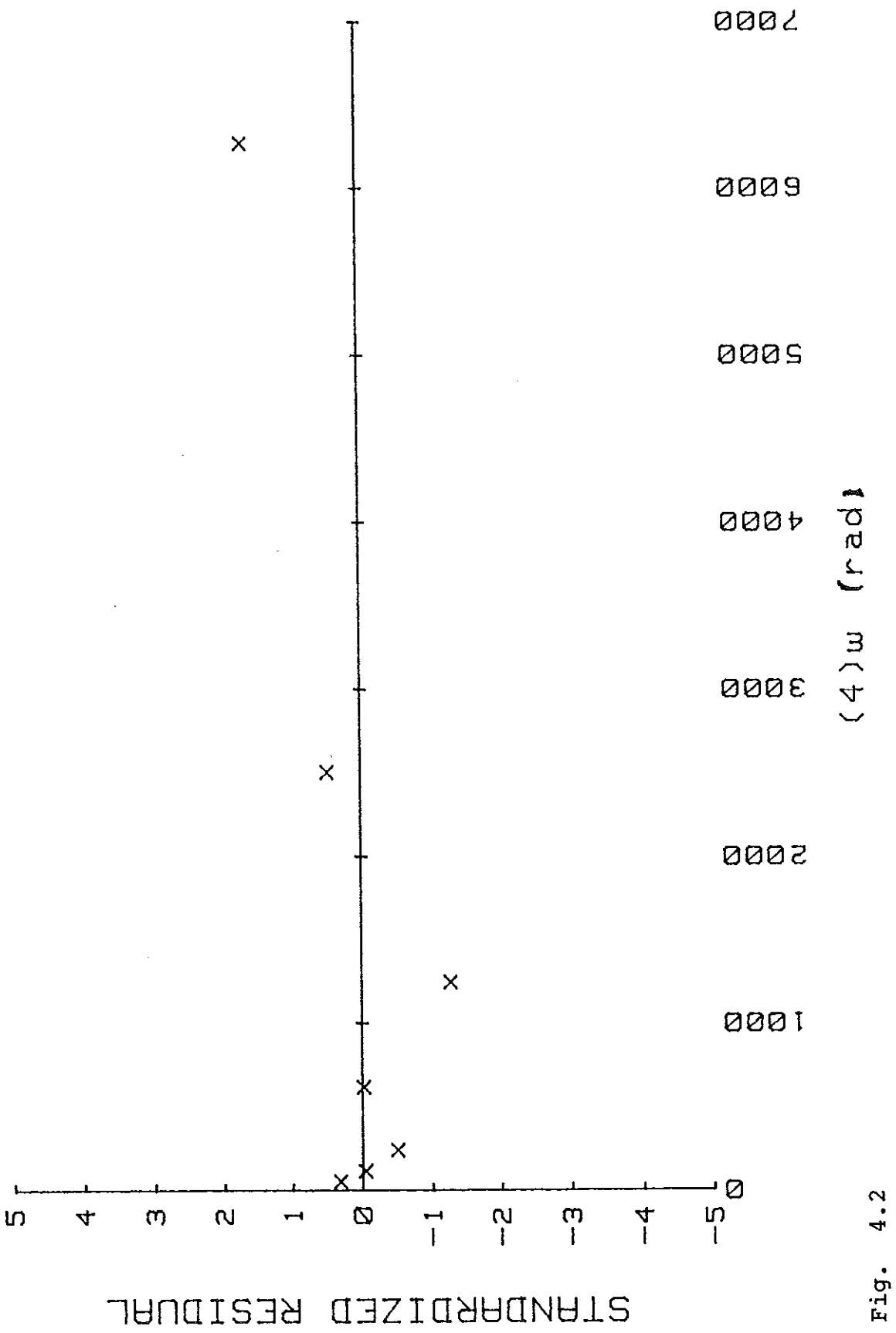
STANDARDIZED RESIDUAL
5
4
3
2
1
0
-1
-2
-3
-4
-5
1000
2000
3000
4000
5000
6000
7000
(4)w (rad)

Fig. 4.2

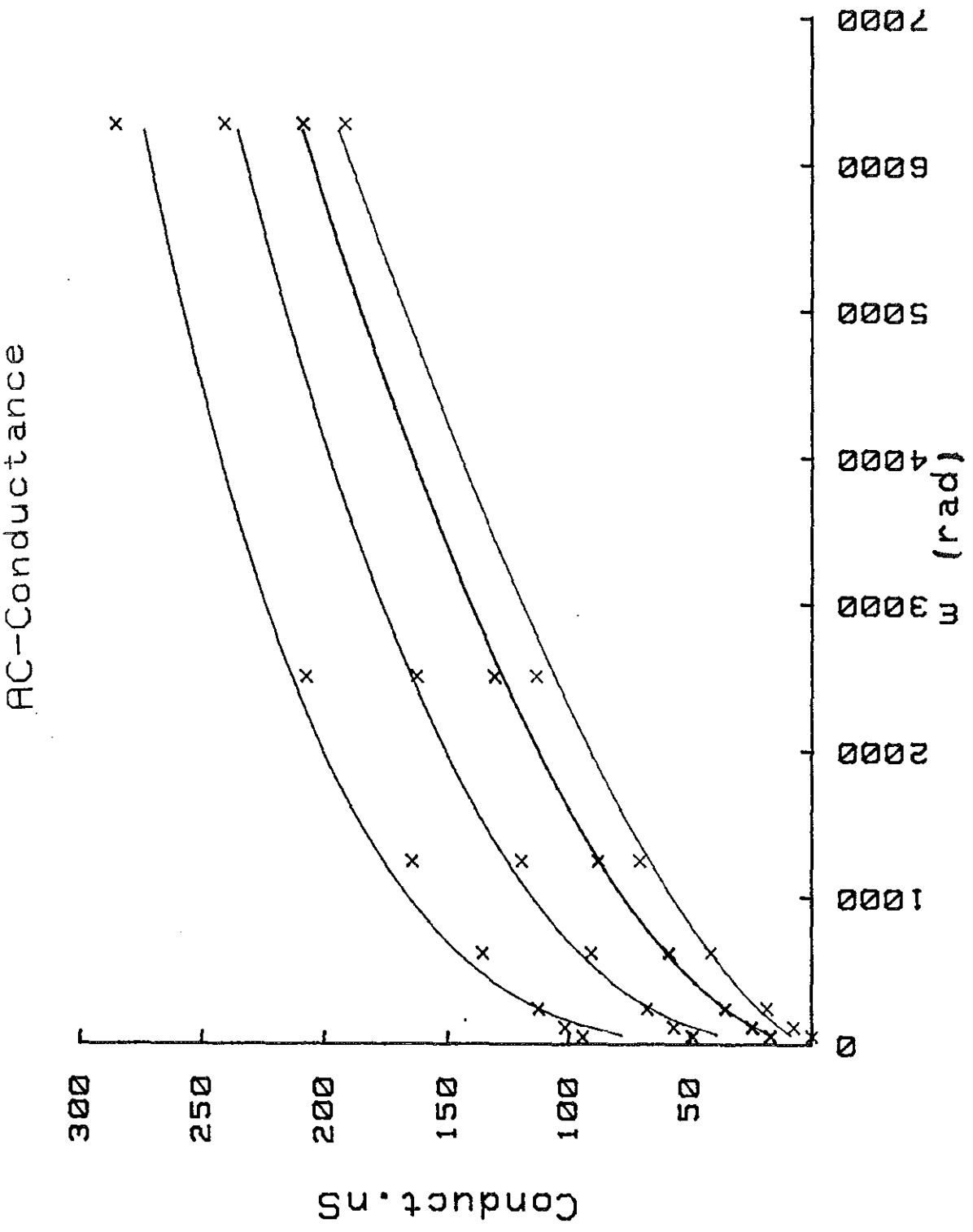
AC-Conductance
Conduct.nS
300
250
200
150
100
50
0
1000
2000
3000
4000
5000
6000
7000
ω (rad)

Fig. 4.3

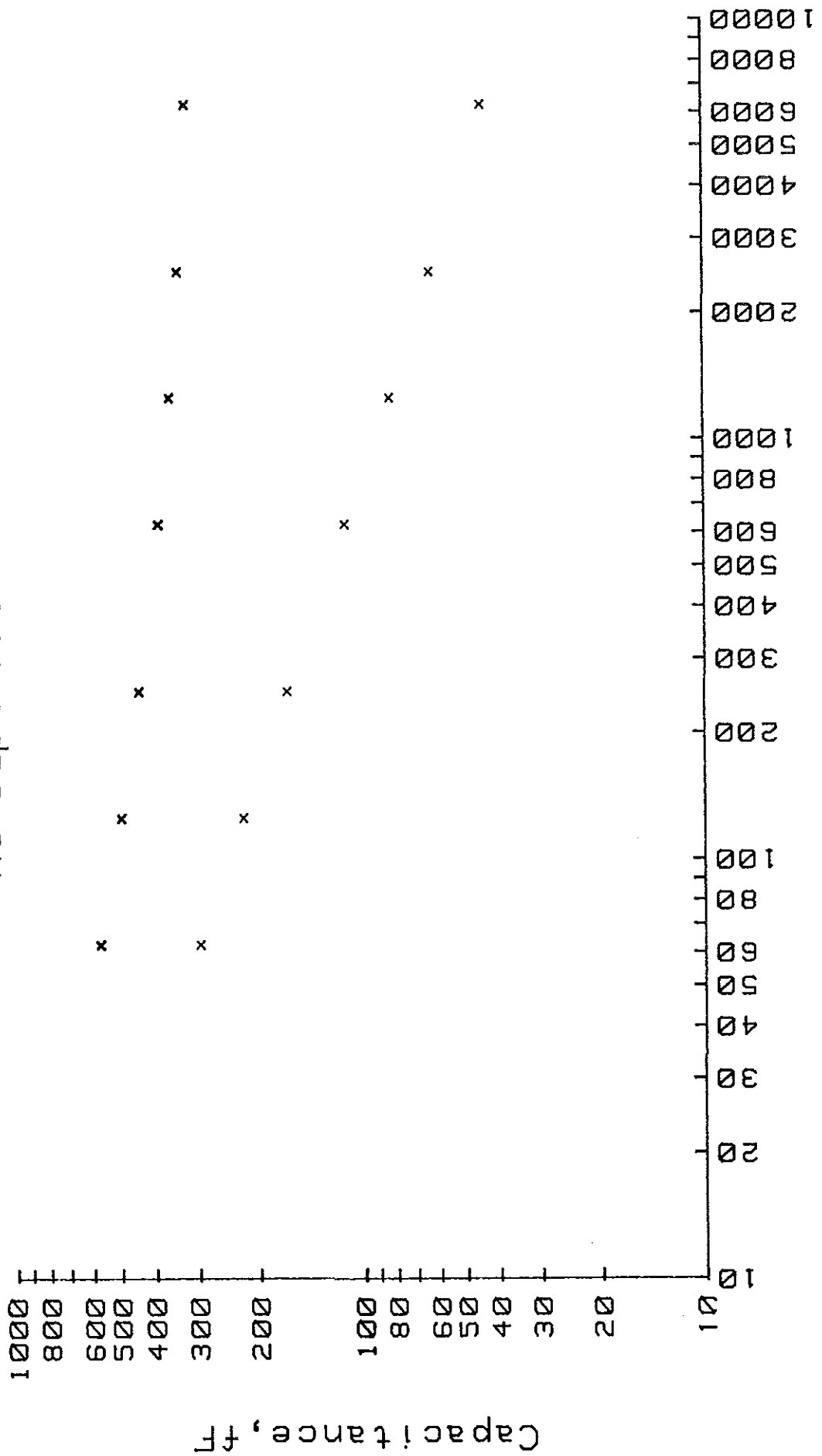

Fig. 4.4 LOG-LOG plot.

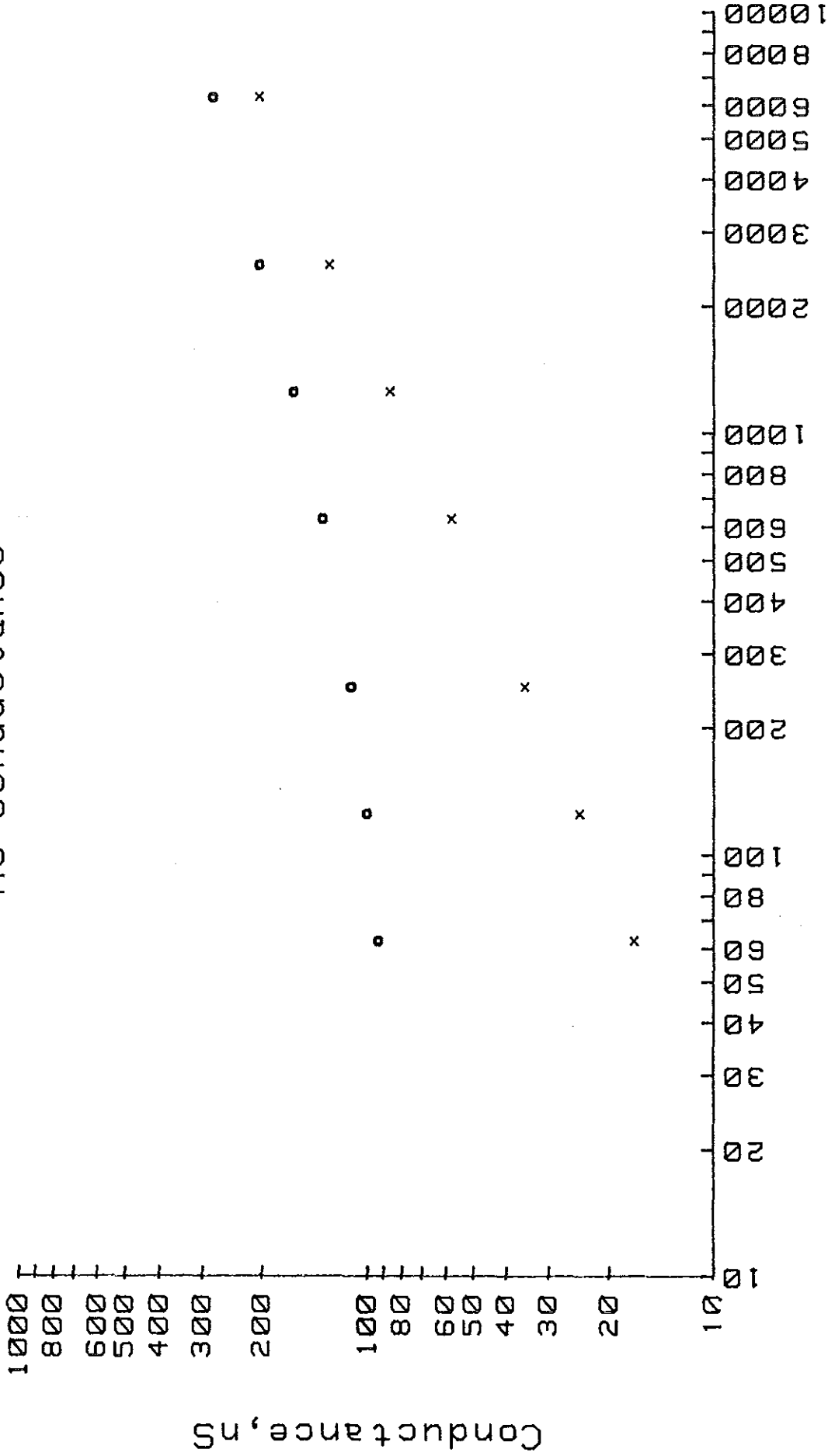

Fig. 4.5 LOG - LOG plot

The value of the frequency exponent S was determined from the fitting of the conductance data and also from the fitting of the ratio (2.24)

$$\frac{\omega Cac}{Gac}$$

which estimates the value for S'-S. Since the value of S' is determined from the fitting procedure of the capacitance, the S'-S value gives the value for S. The value of S determined in both ways is tabulated in table 4 for four measurement temperatures.

The frequency exponent S of conductance was found to decrease with increasing temperature. The plot of S versus T is shown in Fig. (4.6). Comparing Fig.(4.6) with Fig. (2.2) it is clear that the ac loss mechanism is similar to the prediction of the CBH model. Thus using the expression for S in the CBH model (2.18) or (2.8) it is possible to determine the depth of the dominant center for the loss at a particular frequency. As an example from (2.18) we have

$$W_m = \frac{KT\ [6-(1-S)\ \ell n(\omega\tau_o)]}{(1-S)}$$

For T = 443K we have S=.54 (Table 4). Thus for $\omega=2\pi$x100KHZ and $\tau_o = 10^{-11}$S we obtain W_m = 0.95eV. The values of W_m for the case of 100KHZ and $\tau_o \sim 10^{-11}$S at the four temperatures of measurement are tabulated in table 3.

TABLE 4

T	S'-1	S'	S'-S	S	S_o	W_{m1}	W_{m2}
292	-.225	.690	-.125	.82±.02	.725	1.16	1.27
317	-.318	.682	-.116	.80±.04	.671	1.13	1.26
392	-.390	.610	-.039	.65±.08	.605	.99	1.14
443	-.421	.579	..039	.54±.02	.542	.95	1.13

W_{m1} and W_{m2} in eV, respectively, correspond to the cases of 100KHZ and 10KHZ frequencies; S_o determined from the fitting of G.

From the above table it is clear that the depth of the centers that contribute to the loss, at a particular frequency raises with increasing temperature.

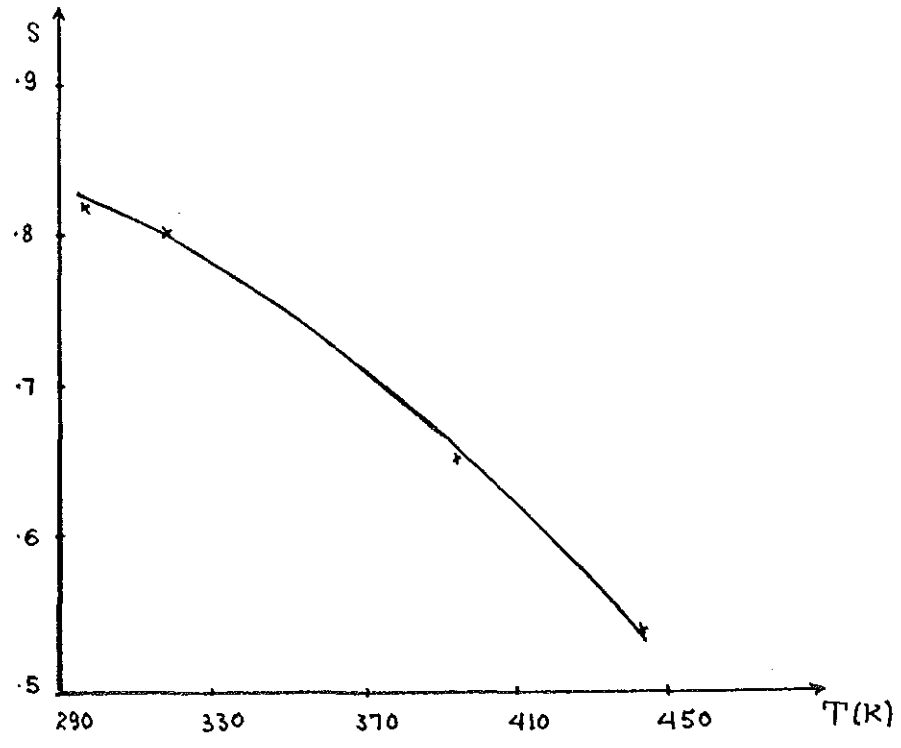

Fig. 4.6 Temperature dependence of the frequency exponent S of the ac conductivity from the experiment on sample UV1Na.

Conclusion

The real and imaginary parts of the ac conductivity as well as the dc conductivity of thin films of hydrogenated amorphous silicon (a-S_iH), prepared by the HOMO CVD method with different conditions have been measured in the frequency range 10^3-10^6 HZ and in the temperature range 296-443K. These films exhibit an ac conductance $G(\omega)$ whose magnitude is rather strongly temperature dependent and whose frequency exponent S is also markedly temperature dependent.

Of the various models for ac conduction in amorphous semiconductors that have been proposed in the literature the correlated-barrier-hopping (CBH) model is consistent with the loss data. Determination of frequency dependent capacitance and conductance allows the determination of dominant centres that contribute to the frequency dependent transport.

The result of temperature dependent conductivity, $\sigma(T)$, measurement shows that there exist localized states in the principal energy gap in all the samples that are prepared in different conditions and with different substrates. This measurement showed that all the samples exhibit the band conduction transport mechanism. The analysis of the obtained data shows that there is a relationship between the technological parameters and activation energy as well as pre exponential term.

From the results of this work it is found that the I-V characteristics of a-S_iH thin films, prepared by the HOMO CVD method, depends on the substrate of the film. The films with corning glass substrate exhibit a linear I-V characteristics at all temperatures considered and thus a corning glass substrate is a good candidate for investigating some properties of a-S_iH films. On the other hand films with Sodium substrate exhibit a temperature and applied voltage dependent nonlinear I-V characteristics. Thus one has to consider the I-V characteristics of a film for higher voltage range and also its temperature dependence in order to select good substrates.

Appendix A

The program 'pA_Tem' is constructed to read and graphically display the temperature variation of the sample under investigation.

```
10    ! PROGRAM 'pA_Tem'
20    OUTPUT 723;"F1RAN4"
30   CALL Graph
40   FOR Pen=2 TO 7
50   PEN Pen
60    FOR I=1 TO 1000
70    ENTER 723;F1
80    B=F1
90    B=B*1000
100   T=2.077267E-1+2.495674E+1*B-2.356293E-1*B^2+2.369867E-2*B^3
110   T=DROUND(T,4)
120   DISP T
130   PLOT I,T
140   WAIT .5
150   NEXT I
160   PENUP
170   NEXT Pen
180   END
190   SUB Graph
200   Left=1
210   Right=1000
220   Top=150
221   Bottom=100
230   OUTPUT 2 USING "#,K";CHR$(255)&"K"
240   GINIT
250   PLOTTER IS CRT,"INTERNAL"
260   GRAPHICS ON
270   VIEWPORT 13,127,30,99
280   WINDOW Left,Right,Bottom,Top
290   GRID (Right-Left)/10,(Top-Bottom)/10
300   FRAME
310   CLIP OFF
320   CSIZE 3
330   LORG 6
340   PEN 3
350   FOR I=Left+(Right-Left)/10 TO Right-(Right-Left)/11 STEP (Right-Left)/10
360   MOVE I,Bottom
370   I=DROUND(I,2)
380   LABEL USING "#,K";I
390   NEXT I
400   LORG 8
410   FOR I=Bottom TO Top STEP (Top-Bottom)/10
420   MOVE Left,I
430   I=DROUND(I,3)
440   IF ABS(I)<1.E-14 THEN I=0
450   LABEL USING "#,K";I
460   NEXT I
470   SUBEND
```

Appendix B

The program 'pA' is constructed for the I-V characteristics investigation in such a way that it is possible to get all information and store the information so that it can be used later on.

```
10    ! PROGRAM 'pA'
20    CLEAR 727
30    OUTPUT 727;"AE"
40    OPTION BASE 1
50    P=4
60    N=101 ! CHANGE!
70    ALLOCATE X(P,N),F(N)
80    DIM A$[30]
90    PRINT DATE$(TIMEDATE),TIME$(TIMEDATE)
100   INPUT "Sample N ?",Z$
110   PRINT "Sample N",Z$
120   INPUT "Range ?",H
130   INPUT "dV/dt",Q
140   INPUT "STEP",A
150   PRINT "dV/dt=";Q,"STEP=";A
160   OUTPUT 723;"F1RAN4"
170   ENTER 723;B
180   B=B*1000
190   T=2.077267E-1+2.495674E+1*B-2.356293E-1*B^2+2.369867E-2*B^3
200      IF T>99.99 THEN
210      T=DROUND(T,4)
220      ELSE
230      T=DROUND(T,3)
240      END IF
250   PRINT "V=";B,
260   PRINT "Temperature=";T
270   PRINT
280   PRINT " N"," V","I"," ","  R"," "," t,C"
290   PRINT
300   OUTPUT 727;"F2RA1I2A1B2L2"!I-V,AUTO,MEDIUM,Va-1,Vb-OFF,Va_LIMIT 1mA.
310   OUTPUT 727;"PS";-H-A;";PT";H+A;";PE";A;";PH2;PU";Q;";"!START, STOP, STEP,
      HOLD TIME,dV/dt.
320   T0=TIMEDATE
330   OUTPUT 727;"W1"!AUTO START for V SWEEP
340   J=0
350   J=J+1
360   ENTER 727;A$
370   X(2,J)=VAL(A$[4,13])
380   X(1,J)=VAL(A$[16,21])
390   X(3,J)=X(1,J)/X(2,J)
400     X(3,J)=DROUND(X(3,J),3)
410     X(1,J)=DROUND(X(1,J),3)
420     X(2,J)=DROUND(X(2,J),3)
430   ENTER 723;F(J)
440   F(J)=F(J)*1000
450   X(4,J)=2.077267E-1+2.495674E+1*F(J)-2.356293E-1*F(J)^2+2.369867E-2*F(J)^3
460      IF X(4,J)>99.99 THEN
470      X(4,J)=DROUND(X(4,J),4)
480      ELSE
490      X(4,J)=DROUND(X(4,J),3)
500      END IF
510   PRINT J,X(1,J),X(2,J)," ",X(3,J)," ",X(4,J)
520   IF A$[2,2]<>"L" THEN 350
```

```
530   CLEAR 727
540   OUTPUT 727;"A6"
550   T1=TIMEDATE
560   PRINT "Time of measurment =";TIME$(T1-T0)
570   INPUT "If  NO STORE,then press '1','Return'",My
580   IF My=1 THEN 630
590   CREATE BDAT "UV2C1_1",INT((8*P*N)/256)+2,256
600   ASSIGN @Fi TO "UV2C1_1"
610   OUTPUT @Fi;X(*)
620   ASSIGN @Fi TO *
630   CALL Graph(Z$,Q,A,T,H)
640   FOR K=1 TO J
650   IF X(1,K)=2.8E-20 OR X(1,K)=-2.8E-20 THEN
660   X(1,K)=X(1,K-1)
670   PEN 4
680   ELSE
690   PEN 2
700   END IF
710   LORG 5
720   PLOT X(1,K),X(2,K)
730   PENUP
740   NEXT K
750   GOTO 630
760   END
770   SUB Graph(Z$,Q,A,T,H)
780   H=DROUND(H,1)
790   Left=-H
800   Right=H
810   INPUT "Ymax",Top
820   OUTPUT 2 USING "#,K";CHR$(255)&"K"
830   GINIT
840   PLOTTER IS CRT,"INTERNAL"
850   GRAPHICS ON
860   VIEWPORT 15,127,25,99
870   WINDOW Left,Right,-Top,Top
880   AXES (Right-Left)/10,Top/10,Left,0
890   FRAME
900   CLIP OFF
910   CSIZE 3.5
920   PEN 5
930   MOVE Left+(Right-Left)/20,Top-Top/8
940   LABEL DATE$(TIMEDATE)
950   MOVE Left+(Right-Left)/20,Top-(Top/8+Top/12)
960   LABEL TIME$(TIMEDATE)
970   MOVE Left+(Right-Left)/20,Top-(Top/8+Top/6)
980   LABEL "Sample N ",Z$
990   MOVE Left+(Right-Left)/20,Top-(Top/8+Top/4)
1000  LABEL "dU/dt=";Q;"STEP=";A
1010  MOVE Left+(Right-Left)/20,Top-(Top/8+Top/3)
1020  LABEL "Temp=";T
1030  CSIZE 3
1040  LORG 5
1050  PEN 3
1060  FOR I=Left+(Right-Left)/10 TO Right-(Right-Left)/11 STEP (Right-Left)/10
```

```
1070  MOVE I,-Top/25
1080  I=DROUND(I,2)
1090  LABEL USING "#,K";I
1100  NEXT I
1110  LORG 8
1120  FOR I=-Top TO Top STEP Top/5
1130  MOVE Left,I
1140  I=DROUND(I,2)
1150  IF ABS(I)<1.E-14 THEN I=0
1160  LABEL USING "#,K";I
1170  NEXT I
1180  SUBEND
```

Appendix C

The program 'pA_I_T' is constructed for the G-T characteristics investigation. It is a modification of the program 'pA'.

```
10    ! PR 'pA_I_T'
20    CLEAR 727
30    OUTPUT 727;"F1RA1I2A5B2" ! I,AUTO,MED,DC,B_Off
40    Volt=10
50    OUTPUT 727;"PA";Volt;";"
60    OUTPUT 727;"W1"
70    OUTPUT 723;"F1RAN4"! DC,AUTO,4 1/2 digits
80    OPTION BASE 1
90    P=5
100   N=100
110   ALLOCATE X(P,N),F(N),Time(N),V(N)
120   INPUT "Sample N ?",Z$
130   PRINT "Sample N ",Z$
140   PRINT "V=";Volt
150   WAIT 300
160   BEEP 1300,.5
170   B=6.4E-2  ! SEPARATION
180   L=4.38E-1 ! LENGTH OF CONTACTS
190   D=1.26E-4 ! THICKNESS
200   Go=B/(Volt*L*D)
210   To=TIMEDATE
220   Q=30*60/100 !30 min
230   FOR J=1 TO N
240   FOR R=1 TO 7
250   V(J)=SQR(700.0*(R+7*(J-1)))+245
260   NEXT R
270   OUTPUT 706 USING "#,4D";V(J)+2000
280   ENTER 727;X(1,J) ! Current
290   IF X(1,J)<0 THEN X(1,J)=1.E-15
300   X(5,J)=X(1,J)*Go ! Conductivity
310   X(1,J)=DROUND(X(1,J),3)
320   X(5,J)=DROUND(X(5,J),3)
330   Time(J)=(TIMEDATE-To)/60
340   X(4,J)=DROUND(Time(J),3)
350   ENTER 723;F(J)
360   F(J)=F(J)*1000
370   X(2,J)=2.077267E-1+2.495674E+1*F(J)-2.356293E-1*F(J)^2+2.369867E-2*F(J)^3
380      IF X(2,J)>99.99 THEN
390      X(2,J)=DROUND(X(2,J),4)
400      ELSE
410      X(2,J)=DROUND(X(2,J),3)
420      END IF
430   X(3,J)=1000/(273+X(2,J))
440   X(3,J)=DROUND(X(3,J),3)
450   PRINT J,X(4,J),X(2,J),X(3,J),X(1,J),X(5,J),DROUND(LOG(X(5,J)),4)
460   WAIT 0
470   NEXT J
480   OUTPUT 706 USING "#,4D";2000
490   INPUT "If NO STORE,then press '1','Return'",My
500   IF My=1 THEN 620
```

```
510   CREATE BDAT Z$,INT((8*P*N)/256)+2,256
520   ASSIGN @Fy TO Z$
530   OUTPUT @Fy;X(*)
540   ASSIGN @Fy TO *
550   INPUT "If plot I(T), then '1'; If plot LOG_G(1/T), then '2'",Ycl
560   IF Ycl=1 THEN 620
570   IF Ycl=2 THEN 1020
580   IF Ycl=3 THEN 820
590   IF Ycl=4 THEN 920
600   IF Ycl=5 THEN 1360
610   IF Ycl=6 THEN 720
620     Left=0
630     Bottom=0
640     Right=150
650     Ko=15
660 CALL Graph(Z$,Volt,Left,Right,Bottom,Ko) ! I(1/T)
670         FOR I=1 TO N
680         PLOT X(2,I),X(1,I)
690         PENUP
700         NEXT I
710         GOTO 550
720     Left=0
730     Bottom=0
740     Right=0*100/60
750     Ko=10
760 CALL Graph(Z$,Volt,Left,Right,Bottom,Ko) ! T(t)
770         FOR I=1 TO N
780         PLOT X(4,I),X(2,I)
790         PENUP
800         NEXT I
810         GOTO 550
820     Left=0
830     Bottom=2.4
840     Right=0*100/60
850     Ko=10
860 CALL Graph(Z$,Volt,Left,Right,Bottom,Ko) ! 1/T(t)
870         FOR I=1 TO N
880         PLOT X(4,I),X(3,I)
890         PENUP
900         NEXT I
910         GOTO 550
920     Left=2.4
930     Bottom=0
940     Right=3.4
950     Ko=10
960 CALL Graph(Z$,Volt,Left,Right,Bottom,Ko) ! LOG_I(1/T)
970         FOR I=1 TO N
980         PLOT X(3,I),LOG(X(1,I))+30
990         PENUP
1000        NEXT I
1010        GOTO 550
1020    Left=2.4
1030    INPUT "Bottom?",Bottom
1040    Right=3.4
1050    Ko=10
```

```
1060 CALL Graph(Z$,Volt,Left,Right,Bottom,Ko) ! LOG_G(1/T)
1070       FOR I=1 TO N
1080       PLOT X(3,I),LOG(X(5,I))
1090       PENUP
1100       NEXT I
1110  INPUT "Once more?",M$
1120  IF M$="Y" THEN 1020
1130     INPUT "X1,X2",Z1,Z2
1140     FOR I=1 TO N
1150     DISP X(3,I)
1160     IF Z1>=X(3,I) THEN
1170     W1=I
1180     Z1=X(3,I)
1190     PRINT "I1=";W1;"X1=";Z1,
1200     GOTO 1230
1210     END IF
1220     NEXT I
1230     FOR I=1 TO N
1240     DISP X(3,I)
1250     IF Z2>=X(3,I) THEN
1260     W2=I
1270     Z2=X(3,I)
1280     PRINT "I2=";W2;"X2=";Z2,
1290     GOTO 1320
1300     END IF
1310     NEXT I
1320     E=8.625E-2*(LOG(X(5,W1))-LOG(X(5,W2)))/(Z2-Z1)
1330     E=DROUND(E,3)
1340     PRINT "E=";E;"eV","    "
1350       GOTO 1130
1360  END
1370                  SUB Graph(Z$,Volt,Left,Right,Bottom,Ko)
1380  INPUT "Ymax",Top
1390  OUTPUT 2 USING "#,K";CHR$(255)&"K"
1400  GINIT
1410  PLOTTER IS CRT,"INTERNAL"
1420  GRAPHICS ON
1430  VIEWPORT 13,127,30,99
1440  WINDOW Left,Right,Bottom,Top
1450  AXES (Right-Left)/Ko,(Top-Bottom)/10,Left,Bottom
1460  FRAME
1470  CLIP OFF
1480  CSIZE 3.5
1490  PEN 5
1500  MOVE Left+(Right-Left)/3,Top-(Top-Bottom)/16
1510  LABEL DATE$(TIMEDATE)
1520  MOVE Left+(Right-Left)/3,Top-((Top-Bottom)/16+(Top-Bottom)/24)
1530  LABEL TIME$(TIMEDATE)
1540  MOVE Left+(Right-Left)/3,Top-((Top-Bottom)/16+(Top-Bottom)/12)
1550  LABEL "Sample #";Z$
1560  MOVE Left+(Right-Left)/3,Top-((Top-Bottom)/16+(Top-Bottom)/8)
1570  LABEL "V=";Volt;"V"
1580  CSIZE 3
1590  LORG 6
1600  PEN 3
```

```
1610  FOR I=Left+(Right-Left)/Ko TO Right-(Right-Left)/(Ko+1) STEP (Right-Left)/
Ko
1620  MOVE I,Bottom
1630  I=DROUND(I,3)
1640  LABEL USING "#,K";I
1650  NEXT I
1660  LORG 8
1670  FOR I=Bottom TO Top STEP (Top-Bottom)/10
1680  MOVE Left,I
1690  I=DROUND(I,3)
1700  IF ABS(I)<1.E-14 THEN I=0
1710  LABEL USING "#,K";I
1720  NEXT I
1730  PEN 2
1740  SUBEND
```

REFERENCES

1. Richard Zallen, "The Physics of Amorphous Solids" Wiley-Interscience publication, 1983
2. P.W. Anderson, 1958, Phys. Rev. 109, 1492
3. N.F. Mott, J. Phys. C. 13 (1980), 5433-71
4. Stephen J. Fonash, "Solar Cell Device Physics" Academic Press, 1981
5. Nevill Mott, Contemp. Phys. 1985. Vol.26, No.3, 203-215
6. A.D. Zdetsis et al 1985, Phys.Rev. B31, No.4, 2410-15
7. R.A. Smith "Semiconductors" Second Edition, Cambridge University Press, 1987
8. Semereab Habtetsion, "experimental Analysis of some properties of Hydrogenated Amorphous Silicon Solar Cell" University of Sheffield, 1986
9. P.G. Lecomber and W.E.Spear, Phys. Rev. Lett.25, 509, 1970
10. David L.Miller, J.Appl. Phys.49, 6192 (1978)
11. Alan L.Fahrenbruch and Richard H.Bube, "Fundamentals of Solar cells" Academic Press, 1983
12. N.Savvides, J.Appl. Phys.56, 2788 (1984)
13. A.K.Ghosh et al, J. Appl. Phys. 50, 3407 (1979)
14. G.H.Dohler, Phys. Rev. B19, No.4, 2083 (1979)
15. Yu.M. Galperin, V.G. Karpov, and V.I.Kozub, Adv. Phys., 1989, 38, No.6, 669-737
16. M. Pollak and T.H. Geballe, 1961, Phys. Rev.122,1742
17. A.R.Long. Adv. Phys., 1982, 31, No.5, 553-637
18. P.Extance, 1985, Phys.Rev. B32, No.12, 8148

19. G.E. Pike, 1972, Phys.Rev. B6, No.4, 1572

20. G.Rieder, 1979, Phys. Rev. B20, No.2, 607

21. A.J.Lewis, 1976, Phys. Rev. B14, 658

22. C.Y.Huang, S.Guha and S.J. Hudgens, 1983, Phys.Rev. B27, No.12, 7460

23. P.B.Kirby and W.Paul, 1984, Phys.Rev. B29, No.2, 826

24. R.E.Lagos, 1983, J.Appl. Phys.54, No.7, 3951

25. A.K. Cheetham and Peter Day, "Solid State Chemistry" 1987, Oxford University Press

26. M. Pollak, 1964, Phys. Rev.A, 133, 564

27. Arthur R.Von Hippel, "Dielectric Materials and Applications" 1954, Massachusets Institute of Technology.

28. Henry Shenker, J.I.Lauritzen, R.J.Corruccini and S.T. Lonberger, "Reference Tables for Thermocouples", National Bureau of standards, 1955

29. H.Frohlich, "Theory of Dielectrics", Oxford Press, 1958

30. S.M.Sze, "Physics of Semiconductor Devices" second edition, John Wiley and Sons, 1981

31. J.S. Blakemore "Solid State Physics" Cambridge University Press, 1985

Declaration

The Thesis is my original work, has not been presented for a degree in any other University and that all sources of material used for the thesis have been duly acknowledged.

MESERET YIFRU _____

Place and date of submission:

This thesis has been submitted for examination with my approval as University Advisor.

Dr. S. Bezludnyi _____

Appendix A

The program 'pA_Tem' is constructed to read and graphically display the temperature variation of the sample under investigation.

```
10    ! PROGRAM 'pA_Tem'
20    OUTPUT 723;"F1RAN4"
30   CALL Graph
40   FOR Pen=2 TO 7
50   PEN Pen
60    FOR I=1 TO 1000
70    ENTER 723;F1
80    B=F1
90    B=B*1000
100   T=2.077267E-1+2.495674E+1*B-2.356293E-1*B^2+2.369867E-2*B^3
110   T=DROUND(T,4)
120   DISP T
130   PLOT I,T
140   WAIT .5
150   NEXT I
160   PENUP
170   NEXT Pen
180   END
190   SUB Graph
200   Left=1
210   Right=1000
220   Top=150
221   Bottom=100
230   OUTPUT 2 USING "#,K";CHR$(255)&"K"
240   GINIT
250   PLOTTER IS CRT,"INTERNAL"
260   GRAPHICS ON
270   VIEWPORT 13,127,30,99
280   WINDOW Left,Right,Bottom,Top
290   GRID (Right-Left)/10,(Top-Bottom)/10
300   FRAME
310   CLIP OFF
320   CSIZE 3
330   LORG 6
340   PEN 3
350   FOR I=Left+(Right-Left)/10 TO Right-(Right-Left)/11 STEP (Right-Left)/10
360   MOVE I,Bottom
370   I=DROUND(I,2)
380   LABEL USING "#,K";I
390   NEXT I
400   LORG 8
410   FOR I=Bottom TO Top STEP (Top-Bottom)/10
420   MOVE Left,I
430   I=DROUND(I,3)
440   IF ABS(I)<1.E-14 THEN I=0
450   LABEL USING "#,K";I
460   NEXT I
470   SUBEND
```

Appendix B

The program 'pA' is constructed for the I-V characteristics investigation in such a way that it is possible to get all information and store the information so that it can be used later on.

```
10    ! PROGRAM 'pA'
20    CLEAR 727
30    OUTPUT 727;"AE"
40    OPTION BASE 1
50    P=4
60    N=101 ! CHANGE!
70    ALLOCATE X(P,N),F(N)
80    DIM A$[30]
90    PRINT DATE$(TIMEDATE),TIME$(TIMEDATE)
100   INPUT "Sample N ?",Z$
110   PRINT "Sample N",Z$
120   INPUT "Range ?",H
130   INPUT "dV/dt",Q
140   INPUT "STEP",A
150   PRINT "dV/dt=";Q,"STEP=";A
160   OUTPUT 723;"F1RAN4"
170   ENTER 723;B
180   B=B*1000
190   T=2.077267E-1+2.495674E+1*B-2.356293E-1*B^2+2.369867E-2*B^3
200      IF T>99.99 THEN
210      T=DROUND(T,4)
220      ELSE
230      T=DROUND(T,3)
240      END IF
250   PRINT "V=";B,
260   PRINT "Temperature=";T
270   PRINT
280   PRINT " N"," V","I"," ","  R"," "," t,C"
290   PRINT
300   OUTPUT 727;"F2RA1I2A1B2L2"!I-V,AUTO,MEDIUM,Va-1,Vb-OFF,Va_LIMIT 1mA,
310   OUTPUT 727;"PS";-H-A;";PT";H+A;";PE";A;";PH2;PV";Q;";"!START, STOP, STEP,
      HOLD TIME,dV/dt.
320   T0=TIMEDATE
330   OUTPUT 727;"W1"!AUTO START for V SWEEP
340   J=0
350   J=J+1
360   ENTER 727;A$
370   X(2,J)=VAL(A$[4,13])
380   X(1,J)=VAL(A$[16,21])
390   X(3,J)=X(1,J)/X(2,J)
400     X(3,J)=DROUND(X(3,J),3)
410     X(1,J)=DROUND(X(1,J),3)
420     X(2,J)=DROUND(X(2,J),3)
430   ENTER 723;F(J)
440   F(J)=F(J)*1000
450   X(4,J)=2.077267E-1+2.495674E+1*F(J)-2.356293E-1*F(J)^2+2.369867E-2*F(J)^3
460       IF X(4,J)>99.99 THEN
470       X(4,J)=DROUND(X(4,J),4)
480       ELSE
490       X(4,J)=DROUND(X(4,J),3)
500       END IF
510   PRINT J,X(1,J),X(2,J)," ",X(3,J)," ",X(4,J)
520   IF A$[2,2]<>"L" THEN 350
```

```
530   CLEAR 727
540   OUTPUT 727;"A6"
550   T1=TIMEDATE
560   PRINT "Time of measurment =";TIME$(T1-T0)
570   INPUT "If  NO STORE,then press '1','Return'",My
580   IF My=1 THEN 630
590   CREATE BDAT "UV2C1_1",INT((8*P*N)/256)+2,256
600   ASSIGN @Fi TO "UV2C1_1"
610   OUTPUT @Fi;X(*)
620   ASSIGN @Fi TO *
630   CALL Graph(Z$,Q,A,T,H)
640   FOR K=1 TO J
650   IF X(1,K)=2.8E-20 OR X(1,K)=-2.8E-20 THEN
660   X(1,K)=X(1,K-1)
670   PEN 4
680   ELSE
690   PEN 2
700   END IF
710   LORG 5
720   PLOT X(1,K),X(2,K)
730   PENUP
740   NEXT K
750   GOTO 630
760   END
770   SUB Graph(Z$,Q,A,T,H)
780   H=DROUND(H,1)
790   Left=-H
800   Right=H
810   INPUT "Ymax",Top
820   OUTPUT 2 USING "#,K";CHR$(255)&"K"
830   GINIT
840   PLOTTER IS CRT,"INTERNAL"
850   GRAPHICS ON
860   VIEWPORT 15,127,25,99
870   WINDOW Left,Right,-Top,Top
880   AXES (Right-Left)/10,Top/10,Left,0
890   FRAME
900   CLIP OFF
910   CSIZE 3.5
920   PEN 5
930   MOVE Left+(Right-Left)/20,Top-Top/8
940   LABEL DATE$(TIMEDATE)
950   MOVE Left+(Right-Left)/20,Top-(Top/8+Top/12)
960   LABEL TIME$(TIMEDATE)
970   MOVE Left+(Right-Left)/20,Top-(Top/8+Top/6)
980   LABEL "Sample N ",Z$
990   MOVE Left+(Right-Left)/20,Top-(Top/8+Top/4)
1000  LABEL "dV/dt=";Q;"STEP=";A
1010  MOVE Left+(Right-Left)/20,Top-(Top/8+Top/3)
1020  LABEL "Temp=";T
1030  CSIZE 3
1040  LORG 5
1050  PEN 3
1060  FOR I=Left+(Right-Left)/10 TO Right-(Right-Left)/11 STEP (Right-Left)/10
```

```
1070  MOVE I,-Top/25
1080  I=DROUND(I,2)
1090  LABEL USING "#,K";I
1100  NEXT I
1110  LORG 8
1120  FOR I=-Top TO Top STEP Top/5
1130  MOVE Left,I
1140  I=DROUND(I,2)
1150  IF ABS(I)<1.E-14 THEN I=0
1160  LABEL USING "#,K";I
1170  NEXT I
1180  SUBEND
```

Appendix C

The program 'pA_I_T' is constructed for the G-T characteristics investigation. It is a modification of the program 'pA'.

```
10    ! PR 'pA_I_T'
20    CLEAR 727
30    OUTPUT 727;"F1RA1I2A5B2" ! I,AUTO,MED,DC,B_Off
40    Volt=10
50    OUTPUT 727;"PA";Volt;";"
60    OUTPUT 727;"W1"
70    OUTPUT 723;"F1RAN4"! DC,AUTO,4 1/2 digits
80    OPTION BASE 1
90    P=5
100   N=100
110   ALLOCATE X(P,N),F(N),Time(N),V(N)
120   INPUT "Sample N ?",Z$
130   PRINT "Sample N ",Z$
140   PRINT "U=";Volt
150   WAIT 300
160   BEEP 1300,.5
170   B=6.4E-2  ! SEPARATION
180   L=4.38E-1 ! LENGTH OF CONTACTS
190   D=1.26E-4 ! THICKNESS
200   Go=B/(Volt*L*D)
210   To=TIMEDATE
220   O=30*60/100 !30 min
230   FOR J=1 TO N
240   FOR R=1 TO 7
250   V(J)=SQR(700.0*(R+7*(J-1)))+245
260   NEXT R
270   OUTPUT 706 USING "#,4D";V(J)+2000
280   ENTER 727;X(1,J) ! Current
290   IF X(1,J)<0 THEN X(1,J)=1.E-15
300   X(5,J)=X(1,J)*Go ! Conductivity
310   X(1,J)=DROUND(X(1,J),3)
320   X(5,J)=DROUND(X(5,J),3)
330   Time(J)=(TIMEDATE-To)/60
340   X(4,J)=DROUND(Time(J),3)
350   ENTER 723;F(J)
360   F(J)=F(J)*1000
370   X(2,J)=2.077267E-1+2.495674E+1*F(J)-2.356293E-1*F(J)^2+2.369867E-2*F(J)^3
380      IF X(2,J)>99.99 THEN
390      X(2,J)=DROUND(X(2,J),4)
400      ELSE
410      X(2,J)=DROUND(X(2,J),3)
420      END IF
430   X(3,J)=1000/(273+X(2,J))
440   X(3,J)=DROUND(X(3,J),3)
450   PRINT J,X(4,J),X(2,J),X(3,J),X(1,J),X(5,J),DROUND(LOG(X(5,J)),4)
460   WAIT 0
470   NEXT J
480   OUTPUT 706 USING "#,4D";2000
490   INPUT "If NO STORE,then press '1','Return'",My
500   IF My=1 THEN 620
```

```
510   CREATE BDAT Z$,INT((8*P*N)/256)+2,256
520   ASSIGN @Fy TO Z$
530   OUTPUT @Fy;X(*)
540   ASSIGN @Fy TO *
550   INPUT "If plot I(T), then '1'; If plot LOG_G(1/T), then '2'",Ycl
560   IF Ycl=1 THEN 620
570   IF Ycl=2 THEN 1020
580   IF Ycl=3 THEN 820
590   IF Ycl=4 THEN 920
600   IF Ycl=5 THEN 1360
610   IF Ycl=6 THEN 720
620     Left=0
630     Bottom=0
640     Right=150
650     Ko=15
660 CALL Graph(Z$,Volt,Left,Right,Bottom,Ko) ! I(1/T)
670         FOR I=1 TO N
680         PLOT X(2,I),X(1,I)
690         PENUP
700         NEXT I
710         GOTO 550
720     Left=0
730     Bottom=0
740     Right=0*100/60
750     Ko=10
760 CALL Graph(Z$,Volt,Left,Right,Bottom,Ko) ! T(t)
770         FOR I=1 TO N
780         PLOT X(4,I),X(2,I)
790         PENUP
800         NEXT I
810         GOTO 550
820     Left=0
830     Bottom=2.4
840     Right=0*100/60
850     Ko=10
860 CALL Graph(Z$,Volt,Left,Right,Bottom,Ko) ! 1/T(t)
870         FOR I=1 TO N
880         PLOT X(4,I),X(3,I)
890         PENUP
900         NEXT I
910         GOTO 550
920     Left=2.4
930     Bottom=0
940     Right=3.4
950     Ko=10
960 CALL Graph(Z$,Volt,Left,Right,Bottom,Ko) ! LOG_I(1/T)
970         FOR I=1 TO N
980         PLOT X(3,I),LOG(X(1,I))+30
990         PENUP
1000        NEXT I
1010        GOTO 550
1020    Left=2.4
1030    INPUT "Bottom?",Bottom
1040    Right=3.4
1050    Ko=10
```

```
1060 CALL Graph(Z$,Volt,Left,Right,Bottom,Ko) ! LOG_G(1/T)
1070       FOR I=1 TO N
1080       PLOT X(3,I),LOG(X(5,I))
1090       PENUP
1100       NEXT I
1110  INPUT "Once more?",M$
1120  IF M$="Y" THEN 1020
1130     INPUT "X1,X2",Z1,Z2
1140     FOR I=1 TO N
1150     DISP X(3,I)
1160     IF Z1>=X(3,I) THEN
1170     W1=I
1180     Z1=X(3,I)
1190     PRINT "I1=";W1;"X1=";Z1,
1200     GOTO 1230
1210     END IF
1220     NEXT I
1230     FOR I=1 TO N
1240     DISP X(3,I)
1250     IF Z2>=X(3,I) THEN
1260     W2=I
1270     Z2=X(3,I)
1280     PRINT "I2=";W2;"X2=";Z2,
1290     GOTO 1320
1300     END IF
1310     NEXT I
1320     E=8.625E-2*(LOG(X(5,W1))-LOG(X(5,W2)))/(Z2-Z1)
1330     E=DROUND(E,3)
1340     PRINT "E=";E;"eV","    "
1350       GOTO 1130
1360  END
1370                    SUB Graph(Z$,Volt,Left,Right,Bottom,Ko)
1380  INPUT "Ymax",Top
1390  OUTPUT 2 USING "#,K";CHR$(255)&"K"
1400  GINIT
1410  PLOTTER IS CRT,"INTERNAL"
1420  GRAPHICS ON
1430  VIEWPORT 13,127,30,99
1440  WINDOW Left,Right,Bottom,Top
1450  AXES (Right-Left)/Ko,(Top-Bottom)/10,Left,Bottom
1460  FRAME
1470  CLIP OFF
1480  CSIZE 3.5
1490  PEN 5
1500  MOVE Left+(Right-Left)/3,Top-(Top-Bottom)/16
1510  LABEL DATE$(TIMEDATE)
1520  MOVE Left+(Right-Left)/3,Top-((Top-Bottom)/16+(Top-Bottom)/24)
1530  LABEL TIME$(TIMEDATE)
1540  MOVE Left+(Right-Left)/3,Top-((Top-Bottom)/16+(Top-Bottom)/12)
1550  LABEL "Sample #";Z$
1560  MOVE Left+(Right-Left)/3,Top-((Top-Bottom)/16+(Top-Bottom)/8)
1570  LABEL "U=";Volt;"V"
1580  CSIZE 3
1590  LORG 6
1600  PEN 3
```

```
1610  FOR I=Left+(Right-Left)/Ko TO Right-(Right-Left)/(Ko+1) STEP (Right-Left)/
Ko
1620  MOVE I,Bottom
1630  I=DROUND(I,3)
1640  LABEL USING "#,K";I
1650  NEXT I
1660  LORG 8
1670  FOR I=Bottom TO Top STEP (Top-Bottom)/10
1680  MOVE Left,I
1690  I=DROUND(I,3)
1700  IF ABS(I)<1.E-14 THEN I=0
1710  LABEL USING "#,K";I
1720  NEXT I
1730  PEN 2
1740  SUBEND
```